Nano Today 25 (2019) 135–155

Contents lists available at ScienceDirect

Nano Today

journal homepage: www.elsevier.com/locate/nanotoday

Review

Biocompatible and biodegradable inorganic nanostructures for nanomedicine: Silicon and black phosphorus

Meng Qiu[a,1], Ajay Singh[b,1], Dou Wang[c,1], Junle Qu[a], Mark Swihart[d], Han Zhang[a,*], Paras N. Prasad[b,e,**]

[a] Shenzhen Second People's Hospital , The First Affiliated Hospital of Shenzhen University and Collaborative Innovation Center for Optoelectronic Science and Technology of Shenzhen University, Shenzhen, 518060, PR China
[b] Institute for Lasers, Photonics, and Biophotonics and Department of Chemistry, University at Buffalo, The State University of New York, Buffalo, NY 14260, USA
[c] Department of Hepatobiliary and Pancreatic Surgery, Shenzhen People's Hospital, Second Clinical Medical College of Jinan University, Shenzhen 518020, Guangdong Province, China
[d] Department of Chemical and Biological Engineering and RENEW Institute, University at Buffalo, The State University of New York, Buffalo, NY 14260, USA
[e] MEPhI, Institute of Engineering Physics for Biomedicine (Phys-Bio Institute), Kashirskoe sh. 31, 115409 Moscow, Russia

ARTICLE INFO

Article history:
Received 9 December 2018
Received in revised form 3 February 2019
Accepted 27 February 2019
Available online 11 March 2019

Keywords:
Silicon
Black phosphorus
Nanomedicine
Biocompatible
Biodegradable

ABSTRACT

Nanomedicine has made great progress toward the diagnosis and treatment of diseases by exploiting physicochemical properties and biological interactions of nanomaterials that differ from the corresponding conventional materials. In the past decade, the advancement of biocompatible and biodegradable inorganic nanostructures has produced numerous nanomedicine platforms. Silicon and, more recently, black phosphorus (BP) offer promising nanoplatforms for bio-applications, including bioimaging, phototherapy, drug delivery, combination therapy, and theranostics, due to their intrinsic unique properties, negligible elemental cytotoxicity, high drug-loading potential, long blood circulation time, and specific clearance pathways. In view of the growing importance of silicon and BP nanomaterials in the progress of nanomedicine, and their common feature characteristics as biodegradable biocompatible elemental semiconductors, this contribution reviews the latest advances in silicon and BP-based biomedical nanomaterials for disease diagnosis and therapy.

Contents

Abbreviations: BP, black phosphorus; FLBP, few-layer black phosphorus; Si, silicon; TMDs, transition metal dichalcogenides; QDs, quantum dots; NSs, nanosheets; NPs, nanoparticles; NIR, near-infrared; PTCE, photothermal conversion efficiency; PTT, photothermal therapy; PDT, photodynamic therapy; PS, photosensitizer; ROS, reactive oxygen species; EPR, enhanced permeability and retention; DDSs, drug delivery systems; MRI, magnetic resonance imaging; NMP, *n*-methyl pyrrolidone; DMSO, dimethyl sulfoxide; DMF, dimethyl formamide; IPA, isopropyl alcohol; CVD, Chemical vapor deposition; PSi, porous silicon; O^{2-}, superoxide anions; CMC, critical micelle concentration; CTAB, cetyltrimethly ammonium bromide; MTT, methyl thiazolyl tetrazolium; CCK-8, Cell Counting Kit-8; TiL_4, titanium sulfonate ligand; RES, reticuloendothelial system; Mb, myoglobin; H_2O_2, hydrogen peroxide; IgG, immunoglobulin G; IFE, inner filter effect; CEA, carcino-embryonic; FET, field-effect transistor; DOX, doxorubicin; FACS, flow cytometry analysis; PCPS, polycation-functionalized nanoporous silicon; RF, radio frequency; BBB, blood-brain barrier; NDs, neurodegenerative disorders.

* Corresponding author at: Collaborative Innovation Center for Optoelectronic Science & Technology, College of Optoelectronic Engineering, Shenzhen University, Shenzhen 518060, China.
** Corresponding author at: Institute for Lasers, Photonics, and Biophotonics and Department of Chemistry, University at Buffalo, State University of New York, Buffalo, NY 14260, USA.
E-mail addresses: hzhang@szu.edu.cn (H. Zhang), pnprasad@buffalo.edu (P.N. Prasad).
[1] These authors contributed equally.

https://doi.org/10.1016/j.nantod.2019.02.012
1748-0132/

Nanomedicine involves the use of nanomaterials with novel or enhanced properties, such as size-dependent tunable electronic, optical, magnetic, and chemical behavior, for medical applications. This field has made great progress in its contributions to biomedical science in the last decades [1–6]. Through innovative design and fabrication of nanostructures, nanomedicine can produce therapeutic agents that target specific sites and cure diseases safely and effectively. Nanomedicine can provide effective photosensitizers for photothermal and photodynamic therapy by producing high photo-thermal conversion efficiency (PTCE) [7–9] and photo-induced reactive oxygen species (ROS) generation [10–12], respectively. Nanostructures can also be developed for bio-imaging technologies in the form of contrast enhancement nanoagents and nanoprobes. For example, nanostructures with broad absorption and narrow emission spectra are valuable for fluorescence imaging [13–17], and magnetic nanomaterials can be used as contrast agents for magnetic resonance imaging (MRI) [18], while nanomaterials with high PTCE can be employed for photothermal imaging and photoacoustic imaging [19–22]. Numerous organic and inorganic nanomaterials have been extensively investigated for nanomedicine, including liposomes, dendrimers, polymer nanoparticles (NPs) and micelles, graphene, carbon nanotubes, metal NPs and quantum dots (QDs). Each kind of nanomaterial has its own merits and limitations. Organic nanomaterials provide broad design flexibility for combining multiple functionalities, but this flexibility is combined with drawbacks including intrinsic design complexity, high manufacturing cost, and structural instability. Inorganic nanomaterials are often intrinsically robust with relatively low manufacturing cost, but their limited design flexibility and functionality present challenges that remain to be fully overcome.

Cytotoxicity and clearance are critical issues for clinical translation of nanomaterials that must be addressed by researchers developing new materials. Many inorganic nanomaterials, and even organic nanostructures, exhibit poor bio-compatibility, and should be coated with biocompatible materials for use in biomedical applications [23]. In addition, they may not degrade *in vivo* and/or be eliminated by renal excretion. Consequently, they may accumulate in particular organs and cause unwanted side effects. Therefore, biocompatible nanomaterials with multiple functionalities are in great demand. Problems associated with long-term accumulation-induced toxicity and incomplete excretion can be overcome by employing silicon nanoparticles (SiNPs) or black phosphorus nanoparticles (BPNPs), which possess distinct advantages of both good biodegradability and bio-compatibility. Elemental silicon, the second most abundant element in the earth's crust, is biodegradable, ecologically safe, and known to be metabolized. Silicon also plays a key role in the growth and maintenance of bones. Silicon degrades *in vivo* to orthosilicic acid, which is the bioavailable form of silicon in the human body and which can be excreted in urine [24,25]. Phosphorus is an essential element accounting for approximately 1% of the total mass of the human body, and its final degradation products are harmless, making BP-based nanomaterial suitable for biomedical applications [8,9,26]. These two elemental semiconductor nanostructures (SiNPs and BPNPs) thus have common features of useful optical, electronic, and chemical properties, biocompatibility, and degradability that lead us to consider them together in this review.

In contrast with many other inorganic nanomaterials, SiNPs and BPNPs have excellent biocompatibility as well as unique physicochemical properties especially suitable for biomedical applications [27–29]. Nanosilicon quantum dots (SiQDs) exhibit bright and size tunable photoluminescence that can be extended to the NIR regime, with excellent photostability for bioimaging applications [17]. In addition, various surface modification strategies enable production of nano-silicon with multiple functions. Silicon nanostructures and silicon-containing nano-formulations, surface-modified with antibodies or aptamers and containing drugs, photosensitizers and genes, can be used for targeted therapy [30]. In combination with contrast agents and fluorophores, SiNPs also provide a powerful tool for multimodal imaging and diagnosis. BP has a tunable direct band gap, and can interact with light from the UV to NIR range [31]. This endows BP with large extinction coefficient, high PTCE and photo-redox capabilities, making BP a potential photosensitizing material for phototherapy [10]. Furthermore, a puckered layer structure held together by van der Waals forces provides BP with an ultra large specific surface area that can be used to load various drugs, bioactive molecules, fluorescent molecules, or metal atoms for applications including targeted drug delivery, cell imaging, tumor therapy, and biomolecular detection [32]. Most importantly, the negligible cytotoxicity and excellent biodegradability make SiNPs and BPNPs particularly suitable candidates for biomedical applications, compared with most other nanomaterials [33,34].

In recent years, great breakthroughs have been achieved in research on SiNPs and BPNPs for a broad range of applications in energy, life sciences, and other fields. In this review, we focus on SiNPs and BPNPs and their related biomedical applications. First,

we discuss the fabrication of SiNPs and BPNPs, including methods used to control their size, shape, thickness and surface functionalization. Secondly, we discuss the multifunctionality achievable with these materials by combining optical, electronic, photochemical, magnetic, and thermal properties. Then, we discuss the toxicity and elimination of SiNPs and BPNPs both *in vitro* and *in vivo*. Furthermore, biomedical applications for disease diagnosis and therapy, including stimuli-responsive drug delivery, phototherapy, and bioimaging are discussed. Finally, we consider the challenges and future prospects that are important for their potential clinical translation.

Fabrication and surface functionalization

Fabrication

The production of few-layer BP has been demonstrated in many research contributions over the past three years. Synthesis approaches can be categorized into top-down (*e.g.* mechanical cleavage and liquid phase exfoliation) and bottom-up (*e.g.* CVD and wet-chemistry) methods [35]. Mechanical exfoliation of BP, exploiting its weak interlayer interaction involving only van der Waals forces, was demonstrated in 2014 [36,37]. The mechanical exfoliation method can be combined with a subsequent plasma thinning process which can produce monolayer or few-layer BP in a controllable manner [38]. However, from the point of view of practical applications, this approach suffers shortcomings such as low yield and lack of morphology controllability. These problems were resolved by the liquid phase exfoliation method, which is a comparatively simpler and less expensive process that can readily be scaled up to meet the needs of bio-applications of few-layer BP. Polar aprotic organic solvents, such as *n*-methyl pyrrolidone (NMP), dimethyl sulfoxide (DMSO), dimethyl formamide (DMF), isopropyl alcohol (IPA), and ethanol have used to prepare few-layer BP [39–41]. In addition, many other methods, *e.g.* ionic liquid solvents to obtain BP at high concentration [42], fast and manageable electrochemical ion intercalation for high efficiency exfoliation [43,44], industrially scalable high shear exfoliation, and microwave assisted exfoliation have been investigated. The use of organic solvents during BP preparation is not conducive to clinical application. To avoid the presence of any residual organic solvents on the BPNP surface, attempts have been made to exfoliate BP in water. However, during the exfoliation process, BP was easily aggregated and rapidly degraded, because of its low stability and high activity in aqueous solution. To solve this problem, Kang et al. attempted surfactant-assisted exfoliation and postprocessing of BP in deoxygenated water. The resulting phosphorene dispersions were stable, highly concentrated and comparable to micromechanically exfoliated phosphorene in structure and chemistry [45]. In addition to the top-down method, a bottom-up method was demonstrated recently. Chemical vapor deposition (CVD), which is capable of controlling the doping content and the thickness of BP, was used to generate an ultra-large few-layer BP sheet with good crystallinity [46,47]. Furthermore, a wet-chemical solvothermal reaction method has also been employed to prepare few-layer BP from bulk red phosphorous precursors [48]. Different strategies and methods of preparation produce distinct nano-morphologies appropriate for various biomedical applications. For example, liquid phase exfoliation can usually produce BP quantum dots (BPQDs) and BP nanosheets (BPNSs) with relatively smaller size in both diameter and thickness. These nanostructures are suitable for bioimaging and drug delivery, due to the influence of quantum confinement effects at small sizes, and the role of size in the EPR effect. On the other hand, CVD-derived BP materials are more appropriate for application in FET-based biosensing, due to the control of doping level and thickness achievable by CVD, to provide better carrier mobility and photoelectronic performance.

Since the first discovery of the unique optical properties of SiNPs [49], various preparation strategies have been proposed to fabricate different types of SiNPs [50]. Bottom–up methods involve condensation reactions of silicon compounds, leading to homogeneous nucleation of nanosilicon in the solid, liquid, or vapor phase. Various physical and chemical means can be used to control nanocrystal nucleation and promote the growth of NPs with uniform morphology. Some of the most effective bottom-up methods of producing SiNPs include solution-phase reduction of chlorosilanes [51], laser pyrolysis of silane [52], low-pressure plasma decomposition of silane [53], and thermal processing of hydrogen silesquioxane [54]. Fabrication of SiNPs by top–down methods normally involves electrochemical etching of silicon wafers in hydrofluoric acid to obtain porous silicon films followed by mechanical grinding or sonication to break the nanoporous film into NPs [29,55–57]. A. H. Kashyout et al. fabricated porous silicon (PSi) by an alkali etching process, in 2 wt% KOH and 15 vol% n-propanol at 80 °C for 5 h [58]. The porous nanosilicon particle size was 15 nm, as calculated from XRD data. The degradation rate of PSi with high porosity was accelerated in acid solution, demonstrating the controllable biodegradability and bioresorbability of PSi. Yet another top-down method involves femtosecond laser ablation of bulk silicon to produce nanosilicon by the rapid heating and vaporization effect of pulsed laser radiation [59]. Use of femtosecond pulses allows control of processing conditions in generation of nanoclusters that, upon interaction with the surrounding environment and one another, form larger NPs. Specific nanoclusters can condense on a substrate in a low-pressure gaseous atmosphere or vacuum to form nanostructured films for biosensing. Pulsed laser ablation in a liquid produces nanoclusters that can form stable colloidal dispersions, as their surfaces are charged. Different preparation strategies produce SiNPs appropriate for different biological applications. For example, SiQDs fabricated by bottom-up methods with uniform size below 10 nm and bright visible photoluminescence have been the most effective for use in bioimaging. On the other hand, porous nanosilicon generated by top–down methods provides tailored pore sizes and volumes and large specific surface area that make it attractive for use in drug delivery.

Surface functionalization

Though bulk BP materials are relatively stable, FLBP degrades by chemical reaction in the presence of water, oxygen and light. Zhou et al. proposed an ambient FLBP degradation mechanism based upon electronic structure calculations and molecular dynamics simulations [60], in which superoxide anions (O_2^-) generated on the FLBP surface under ambient light dissociate and react with phosphorus on the FLBP surface to produce two P—O bonds. Then water molecules interact with the surface oxygen through hydrogen-bonding interactions to remove the phosphorus clusters and break the phosphorene layer. Therefore, surface modification is critical for improving BP stability. On the other hand, because there is no reactive organic functional unit on the BP surface, surface modification of BP for further applications has been challenging. PEGylation has been implemented to overcome this issue [9], but was found to be vulnerable to external interference including biomolecule adsorption and self-aggregation and degradation at high ionic strength. In 2016, Zhao et al. introduced sulfonic ester-ligated titanium onto BP by surface coordination to prepare BP@TiL_4 and found that its stability in aqueous environments was markedly enhanced (Fig. 1A) [61]. Ryder et al. also introduced aryl diazonium covalently bonded to the BP surface, and found that it successfully suppressed the degradation process even for several weeks at ambient conditions (Fig. 1B) [62]. Shao et al. reported preparation of biodegradable BPQD/PLGA nanospheres by encapsu-

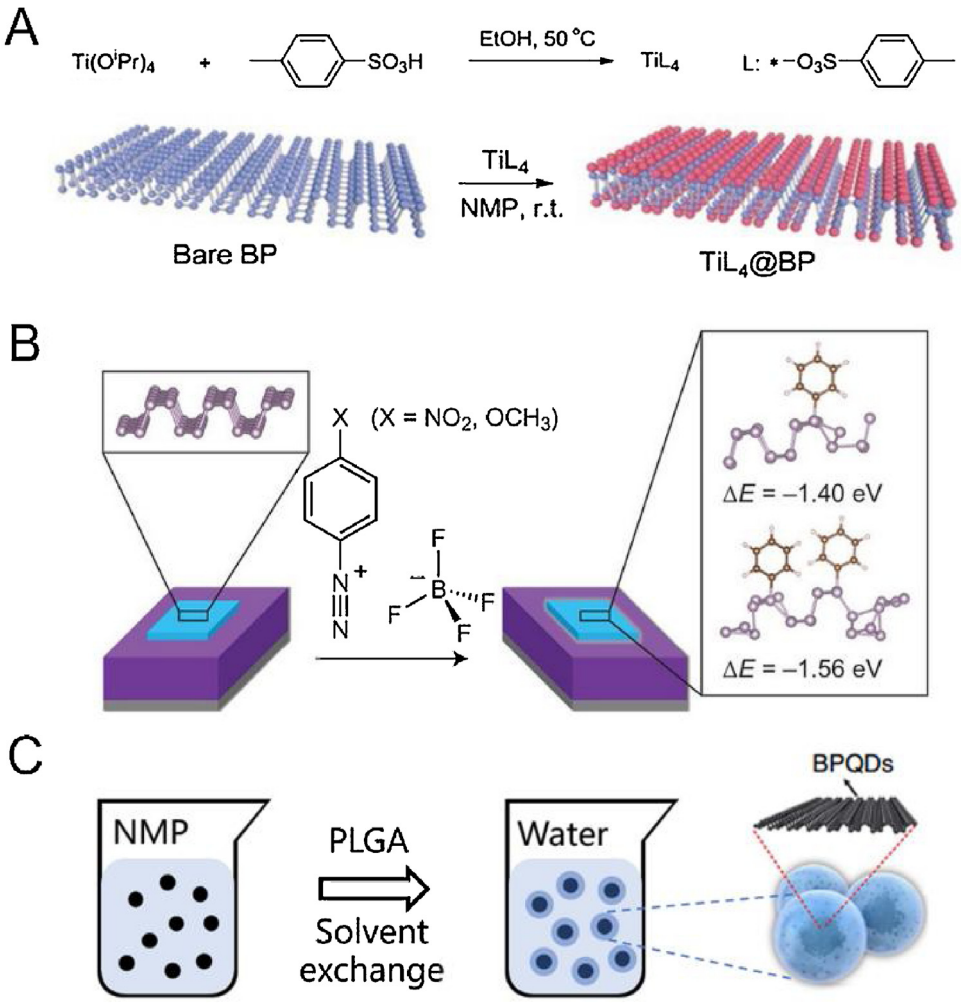

Fig. 1. Various surface functionalization strategies for BP. BP materials (A) Coordinated with sulfonic ester ligated titanium. Images reprinted with permission of [61] © 2016 Wiley-VCH Verlag GmbH & Co. KGaA, Weinheim. (B) Covalently bonded with aryl diazonium. Images reprinted with permission of [62] © 2016 Nature Publishing Group. (C) Coated with PLGA. Images reprinted with permission of [8] © 2018 Nature Publishing Group.

lation of BPQDs into PLGA, and the nanospheres showed a uniform spherical morphology with enhanced stability for more than four weeks (Fig. 1C) [8]. Furthermore, the biodegradation behavior of BPQDs/PLGA nanospheres was accelerated after the PLGA shell was first degraded. In addition to its protective effect, surface modification can also improve the biocompatibility and both electronic and optical properties of BP, which could contribute to its potential in biomedical applications. For example, TiL_4-coated BP could escape macrophage uptake, thus reducing cytotoxicity and proinflammation compared with bare BP [63]. BP modified with the Nile Blue dye through diazonium chemistry exhibited NIR fluorescence, enabling NIR imaging-guided PTT [64]. Functionalization of BP with aryl diazonium further alters its electronic properties, *via* p-type doping which could improve mobility and on/off current ratio in field-effect transistors [62].

The intrinsic biodegradability of SiNPs is generally advantageous for the design of biocompatible formulations for *in vivo* applications. However, bare SiNPs are relatively rapidly degraded to silicic acid in water, particularly under acidic conditions, and this degradation must be slowed for some applications. The relatively low stability of SiNPs under physiological conditions has hindered some bio-applications. Therefore, fabrication of SiNPs that have ability to withstand a physiological environment and maintain their optical and electronic properties long enough to serve their intended purpose, but that still biodegrade and clear from the body at longer times, is essential. Degradation of porous SiNPs has been slowed by surface oxidation or SiO_2 coating [65]. In some cases, organic passivation of SiNP surfaces has been so robust that the particles did not degrade over a period of months *in vivo*. This illustrates the need to achieve an optimal degree and type of passivation of the SiNP surface to control degradation [24]. SiNPs are most often surface passivated *via* a hydrosilylation reaction with an alkene or alkyne that creates a very stable silicon-carbon bond attaching an organic ligand to the SiNP surface [66]. Direct attachment of hydrophilic molecules to the Si surface to promote aqueous dispersibility has been demonstrated [67–69], but has provided limited success in achieving long-term chemical and colloidal stability. Wrapping or encapsulation with polymers improves the water dispersibility of SiNPs, and protects them from aggregation and oxidation [17]. Amphiphilic polymers can form very stable micelles that localize multiple SiQDs in the hydrophobic core region of micelle, which enables co-encapsulation with various hydrophobic cargos [70]. PEGylated micelles encapsulating SiNPs possess excellent stability as well as long circulation time in biological environments [25]. After being surface modified with peptides, aptamers, antibodies or proteins, SiQD formulations can be further endowed with specific targeting ability, which leads to enhanced cell uptake and accumulation in pathological tissue. In one study, myristic acid and SiQDs were co-encapsulated by DSPE-PEG-NH_2 and Pluronic® F127 [30]. Then, CD44-targeting

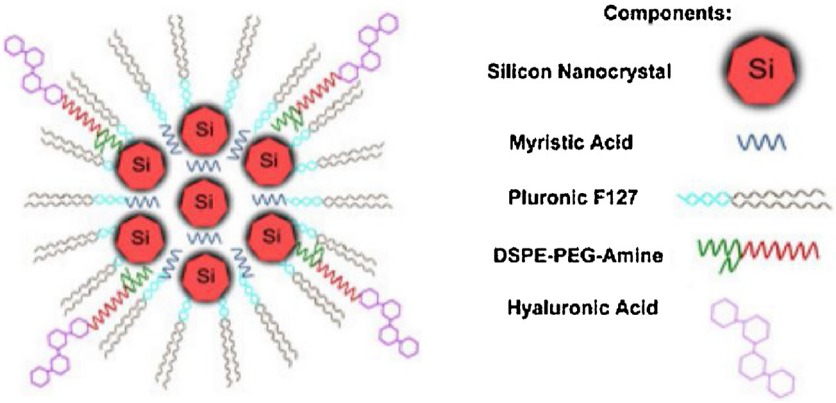

Fig. 2. Schematic of a theranostic nanoformulation of SiNPs. Images reprinted with permission of [30] ©2013 Ivyspring International Publisher.

hyaluronic acid was conjugated to the amine groups of DSPE-PEG-NH_2 (Fig. 2). The myristic acid in the core region of the nanoparticle was released from the micelle over an extended period of time. Further, pluronic® block copolymers were used to encapsulate SiQDs to enhance their water dispersibility for bioimaging. The micelles were formed by the interplay of the poly (oxypropylene) (PPO) section of the F127COOH and the ethyl undecylenate layer around the SiQDs [71]. Consequently, the hydrophilic carboxylate groups at the ends of the F127COOH poly (oxyethylene) (PEO) domain were exposed, providing good dispersibility in aqueous solution. Such polymeric micelles have better stability and lower critical micelle concentration (CMC) values ($\tilde{1}0^{-6}$ M), compared to micelles prepared from traditional small molecule surfactants or detergents, such as sodium dodecyl sulfate (SDS) or cetyltrimethly ammonium bromide (CTAB). Normally, polymeric micelles can encapsulate hydrophobic NPs, providing broad biodistribution, extended systemic circulation time, and reduced toxicity. Surface modification can also have significant impact on the electronic and optical properties of SiNPs. Capping of SiNPs with nitrogen-containing ligands was reported to cause a blue shift of emission wavelength while increasing PL quantum yield to nearly 90% [72,73]. However, these effects depend upon the nature of the initial SiQDs, as demonstrated in a comparison of PL from SiQDs prepared by different synthesis methods interacting with nitrogen-containing molecules [74,75]. In addition, the stability of PL from SiQDs has been a major barrier to commercial applications. Various organic molecules, including Grignard reagents, alkenyl and alkyl functionalities, can provide effective means of stabilizing the luminescence, as discussed in the review by Dasog et al [76].

Fundamental properties

Electronic structure

BP is a direct band gap semiconductor in which the band topology remains the same for all thicknesses, in contrast to the indirect-to-direct band gap transition observed in transition metal dichalcogenides (TMDs). The band gap of bulk BP is 0.3 eV, and the band gap gradually increases to 2.0 eV as the thickness decreases to a single monolayer, due to the quantum confinement effect. For application in transistors, BP not only has a suitable band gap between those of graphene and TMDs, and possesses a moderate on/off ratio ($10^4\tilde{1}0^5$), but also provides a relatively high carrier mobility of around 1000 $cm^2\ V^{-1}\ s^{-1}$. Accordingly, phosphorene has balanced performance that can be extensively utilized for potential photonic and optoelectronic applications, compared with other 2D materials.

Unlike BP, bulk silicon is an indirect bandgap semiconductor, which means its valence band maximum and conduction band minimum have different momentum vectors, and any electronic transition requires participation of a phonon. This requirement drastically reduces the probability of radiative transitions (absorbance and emission of photons) in bulk silicon. However, for SiQDs the momentum selection rule is relaxed as the transitions are localized. At the same time, confinement of photogenerated excitons to a single defect-free and well-passivated nanocrystal reduces the probability of non-radiative recombination. As a result, these SiQDs can be made highly emissive. In addition, because of quantum confinement, the emission wavelength is size dependent. Thus, larger size SiQDs can emit in the near IR, near the bandgap of bulk silicon ($\tilde{1}$.1 eV or $\tilde{1}$100 nm), which falls in the first window of maximum optical transparency in a biological medium, making them very suitable for optical bioimaging.

Optical properties

Because of its layer-dependent electronic band gap, monolayer to few-layer BP covers a wide absorption spectrum and has a strong interaction with electromagnetic waves from the ultraviolet to the mid-infrared range. The layer-dependent band gap tunability of BP is potentially suitable for many optoelectronic applications. BP also exhibits a layer-dependent photoluminescence spectrum due to quantum size effects, which can potentially be used for bioimaging. Castellanos Gomez et al. reported that the photoluminescence of few-layer black phosphorus (FLBP) flakes strongly depends on their thickness. Thinner flakes have an intense peak at 775 nm, while thicker flakes are featureless. Zhang et al. also observed highly layer- and direction-dependent photoluminescence in FLBP. The photoluminescence intensity increases exponentially as the layer thickness decreases from five to two layers.

The photoluminescence of SiQDs arises from recombination of quantum confined charge carriers, and becomes significant when the size of the NPs is comparable to or less than the exciton Bohr radius of silicon. In this regime, both the photoluminescence wavelength and lifetime are dependent on the NC diameter. Tuning the emission wavelength allows one to either use existing filter sets for organic dyes (for particles with emission at visible wavelengths) or to use more deeply penetrating infrared wavelengths. For example, researchers have prepared NIR SiQDs with narrowed emission spectra for deep tissue imaging by controlling NP size [24]. The relatively long photoluminescence lifetime (typically many microseconds) also allows time-gated imaging with a pulsed illumination source to eliminate effects of autofluorescence from biological materials. Silicon is easily oxidized, and in some cases, formation of an oxide layer can greatly impact the

optical property of SiNPs. For example, Park et al. prepared SiNPs by electrochemical etching of single crystalline silicon, and found that the luminescence was activated by silicon oxide grown on the hydrogen-terminated SiNPs, due to the quantum confinement effects and defects at the Si-SiO_2 interface [55]. In other cases, researchers have taken great care to exclude oxygen during surface modification by hydrosilylation, producing nearly oxide-free SiNPs [77,78]. Limiting surface oxidation is particularly important for achieving high PL quantum yield from SiQDs at red and NIR wavelengths [79–81].

Photothermal effect

The photothermal effect involves local conversion of optical energy (*e.g.*, from a laser) to thermal energy *via* photoexcitation of a photosensitizer (PS) that absorbs strongly at the optical wavelength used. Due to its operational simplicity, wide variety of materials available as photosensitizers, and high energy-conversion efficiency, photothermal conversion has garnered renewed research interest in the past decade. It is now used in niche applications, including steam generation, water desalination, and cancer therapy as well as in simpler devices such as solar water heaters. Compared to other PSs for PTT, such as graphene and AuNPs, BP has a very high PTCE, due to its large extinction coefficient and strong nonradiative relaxation derived from phonon interactions in BP crystals. In 2015, Sun et al. first reported that BP exhibits excellent NIR photothermal performance with a large extinction coefficient of 14.8 L g^{-1} cm^{-1} at 808 nm, a photothermal conversion efficiency of 28.4%, and good photostability [9]. Many essential bio-applications including photothermal and photoacoustic imaging as well as photo thermal therapy are based on the remarkable optical absorbance and nonradiative properties of BP.

Biocompatibility and bioavailability

Biocompatibility is widely viewed as the first consideration for biomedical nanomaterials. Any new material must undergo rigorous biological toxicology tests prior to clinical application. However, systematic research on the toxicity of BP is currently quite limited. Only a few studies have examined the cytotoxicity of BP, using a methyl thiazolyl tetrazolium (MTT) assay or a Cell Counting Kit-8 (CCK-8) assay. For instance, H. Zhang et al. reported that after incubation of BPQDs with HSC, C6, 293 T, and MCF7 cells for 48 h, no obvious cytotoxicity was observed for BPQDs concentrations up to 200 ppm [9]. H. U. Lee et al. found that the BP nanodots exhibited low cytotoxicity against COS-7, HeLa, and CHO-K1 cells at a high concentration of 1.0 mg/mL [13]. M. Qiu et al. performed cytotoxicity evaluations at various concentrations of BPNSs, showing that little or no cytotoxic effects could be observed for MDA-MB-231, A549, HeLa, and B16 cells, even at a high concentration of 200 μg/mL of BPNSs [82].

On the contrary, Mo et al. demonstrated that BPNSs and BPQDs produced slight cytotoxic effects on H1299, L0-2, 293 T, dTHP-1 cells, and macrophages in peripheral blood. When BPNSs and BPQDs were coated with a protein corona, the cytotoxic effect was significantly reduced [83]. In another study, BPNSs were also found to reduce A549 cell viability to 48% (WST-8 assay) and 34% (MTT assay) at a concentration of 50 μg/mL, with generally intermediate toxicity between graphene oxides and TMDs [34]. Zhang et al. evaluated the cytotoxicity of BP by a label-free real-time cell analysis technique, which provided concentration, size, and cell type-dependent cytotoxicity (Fig. 3) [84]. The larger BP exhibited greater toxicity, and the smallest BP showed moderate toxicity. The cytotoxicity of BP against 293 T, NIH 3T3, and HCoEpiC cell lines also varied considerably. The possible mechanisms for cytotoxicity were generation of ROS and disruption of cell membrane integrity. Given the contradictory results in the literature, both the degree and mechanisms of inherent cytotoxicity of BP remain uncertain.

Given that current understanding of the biological effects of BP is extremely limited, the actual biological effect of BP *in vivo* is even more difficult to identify. The *in vivo* toxicity of BP was examined in very few studies. Li et al. reported good histocompatibility of BP *in vivo*. Their results showed that intravenous injection of 100 μg BP per mouse caused no apparent side effects or histological changes [19]. Qu et al. investigated biological effects of BP with or without titanium sulfonate ligand (TiL_4) modification *in vitro* and *in vivo* [63]. They found that the bare BP caused an obvious decrease of ATP level in J774 A.1 cells. In addition, the bare BP triggered a series of inflammatory reactions characterized by significant elevation of inflammatory cytokines in mice. In contrast, BP modified with TiL_4 (TiL_4@BP) could surprisingly escape phagocytosis by macrophages, which reduced cytotoxicity and generation of proinflammatory cytokines *in vivo*. These findings provide a new effective method to improve the biocompatibility of BP by surface modification.

Rapid biodegradation is another important advantage of BP for usage *in vivo*. Compared with conventional nanomaterials such as carbon nanomaterials and metal nanostructures, BP-based nanomaterials have advantages in biomedical applications, because of their degradability and inherent biocompatibility, as *P* is an essential element of the human body, accounting for about 1% of total body mass [26]. Unlike graphene, the elemental atoms of BP are connected by weak forces and can react with water and oxygen, and then finally be degraded to various nontoxic phosphates and phosphonates. The biodegradation process of BP is influenced by its size, surface modification and exposure to NIR irradiation. In Shao's research [8], BP/PLGA composites showed a much slower degradation rate compared to a BP nanosheet because of the protection provided by PLGA. Nonetheless, nearly 80% of the BP/PLGA degraded within 8 weeks *in vitro*. Systematic and long-term biosafety evaluations of BP should still be conducted to establish a solid foundation for safe employment of BP-based nanosystems in biomedical applications.

SiQDs can be modified with FDA-approved components for biomedical applications [71]. Silicon is an essential element and widely distributed in living organisms in the form of orthosilicate ions (SiO_4^{4-}). Furthermore, in biological media, silicon nanostructures eventually degrade into orthosilicic acid $Si(OH)_4$, which is naturally excreted through urine. Extensive studies on the cytotoxicity of silicon nanostructures have demonstrated their low toxicity. Kabashin's group confirmed the negligible toxicity of laser ablation-synthesized SiNPs both *in vitro* and *in vivo* [85]. Intravenous administration of SiNPs did not cause any changes in blood chemistry or other key biochemical parameters. Furthermore, they systematically investigated the biodistribution and elimination of SiNPs by quantifying silicon concentration in feces, urine, spleen, lungs, brain, liver, heart and kidneys. SiNPs were opsonized (coated with opsonins) after intravenous injection, which facilitated their clearance from the blood into the reticuloendothelial system, notably the liver and spleen. By 3 to 5 days after injection, SiNPs were degraded and then excreted *via* renal filtration.

Others have reported that the toxicity of SiNPs depends on their size. Zuilhof et al. found that smaller silicon NPs give rise to toxicity, due in part to increased surface area [86]. The cytotoxicity of silicon also depends on the functional groups coated on SiNPs, because different functional groups possess distinct characteristic chemical reactivities. Positively charged capping molecules are more toxic as they could facilitate cell uptake and then reduce metabolic activity [87]. These studies demonstrated the significance of choosing SiNPs of appropriate size and surface functionalization for biomedical applications. Researchers also have evaluated *in vivo*

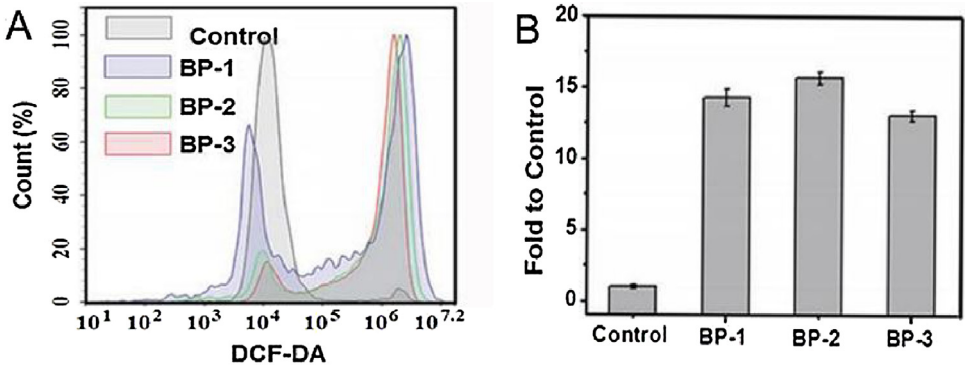

Fig. 3. Analysis of the cytotoxicity of BP *in vitro*. (A–B) Intracellular ROS detection *via* DCF-DA staining and fluorescence intensity analysis by flow cytometry. Images reprinted with permission of [84]. © 2017 Wiley-VCH Verlag GmbH & Co. KGaA, Weinheim.

cytotoxicity in mice for SiQDs of varied particle size and surface functionalization. The result suggests that SiQDs are nontoxic at a dosage of 380 mg kg^{-1} [88]. Further *in vivo* toxicity studies were also extended to monkeys [24]. Monkeys showed no signs of acute toxicity over a 3 month period after injection with a dose of 200 mg kg^{-1} SiNPs, as confirmed by blood chemistry and histology of organs. However, in this study, the SiQDs were protected by a dense, covalently-bound layer of organic ligands on their surface that slowed or prevented their degradation. In summary, SiNPs can be regarded as biocompatible materials and show great potential in clinical applications, but their surface chemistry must be controlled to provide the stability needed for any particular application while still allowing eventual degradation and clearance.

Bioavailability is the second concern that should be addressed when considering the biomedical potential of a nanomaterial. Some researchers have shown that the biodistribution of nanomaterials correlates with size. The enhanced permeation and retention (EPR) and tumor targeting of nanomaterials are most effective for hydrodynamic diameters ranging from 20 to 200 nm [89,90]. Sun et al. performed *in vivo* photoacoustic imaging (PAI) with titanium ligand modified BPQDs (TiL_4@BPQDs) to evaluate their *in vivo* biodistribution [20]. The PA signals reached a maximum at 4 h after TiL4@BPQDs injection, which was 6 times the pre-injection signal intensity. The signal then gradually decreased, and at 48 h postinjection was similar to the preinjection signal. These results indicated that ultra-small BPQDs (~10 nm) tended to suffer from short blood circulation half-life, attenuated EPR effects, reduced tumor accumulation and rapid renal filtration. In another study, when the researchers increased the size of BPQDs/PLGA to 100 nm diameter, considerable fluorescence from the BP nanospheres could be detected at the tumor site at 1 h post-injection. The fluorescence gradually increased for 24 h, demonstrating slower clearance, a good EPR effect, and tumor accumulation of BP nanospheres (Fig. 4A-E) [8]. Fluorescence at the tumor site remained strong at 48-hours post-injection, which indicated good retention of the nanospheres in the tumor.

When the BP nanomaterial reaches a tumor site, it could interact with cell membranes and enter the tumor cells by a cellular uptake pathway. Mei's research group reported that the cellular uptake of BPNSs is mainly through caveolae-dependent endocytosis and micropinocytosis [32]. BP could be transported *via* the "micropinocytosis late endosomes lysosomes" pathway, which can be verified by detecting colocalization between caveolae and DsRed-Rab5 or DsRed-Rab7, which are the markers of early endosomes and late endosomes, respectively (Fig. 4F). In order to promote targeting and uptake efficiency, they further modified PEGylated BPNSs with folate to achieve better tumor targeting through the specific binding between folate and the folate receptors that are overexpressed on cancer cells. The cellular fluorescence intensity in HeLa cells after 1 h of incubation with modified BPNSs was detected by quantitative flow cytometry, and was significantly higher for the folate-modified BPNSs than for the PEGylated BPNSs without folate (Fig. 4G-H). The results of *in vivo* experiments agreed with the *in vitro* study. At 12 h post-intravenous injection of BP/Cy7 NSs and BP-folate/Cy7 NSs, a stronger signal was detected in the tumor of the BP-folate/Cy7 NSs group than in the BP/Cy7 NSs group, further demonstrating that folate targeting is feasible for *in vivo* applications.

The imaging or targeted therapy applications of SiNPs usually require conjugation of a biologically active molecule to the surface to achieve selective and efficient binding or uptake, and often involves encapsulation of the SiQDs in polymer micelles. Researchers have attached biomolecules including folate and antimesothelin directly to SiQDs [91]. These results showed that as-prepared SiNPs possess desirable surface chemistry and selective uptake into Panc-1 cells. In other studies, they passivated the SiQD surface with a hydrophobic ligand layer, and then encapsulated the SiQDs in the hydrophobic core of a PEGylated phospholipid micelle [26,38]. They further combined the SiQDs with the superparamagnetic iron oxide NPs to improve the cellular uptake efficiency [70]. A magnet was placed under the macrophage cell culture dish, and the cells were incubated with the magnetic SiQD nanostructures to demonstrate magnetic guidance capabilities. The result indicated that the iron oxide NPs could increase the cellular uptake of SiQDs under an applied magnetic field. Thus, SiQD-based nanocarriers might be extended to serve as a multimodal guided platform for imaging and traceable drug delivery for cancer therapy, which will minimize damage to normal tissues.

In order to understand more about the SiNP behavior at the cellular level and their intracellular localization, researchers also incubated U87-MG cells with SiNPs. TEM analysis showed that SiNPs appeared mainly inside the cytoplasmic vesicular compartments, where they further formed agglomerates [92]. As SiNPs appeared in endocytotic vesicles and were never visualized inside the nucleus, SiNPs probably enter the cells by endocytosis, a common mechanism for cell uptake of inorganic NPs, and accumulate in lysosomes.

Imaging and sensing

Optical imaging

In recent decades, bio-imaging has drawn great attention for imaging-guided therapy. Quantum dots (QDs) can be ideal for optical bioimaging owing to their broad excitation spectrum combined with narrow and size-dependent emission peaks. However, most widely investigated QDs are cadmium based, and therefore suffer from the risk of toxicity associated with cadmium. Recently, BPQDs

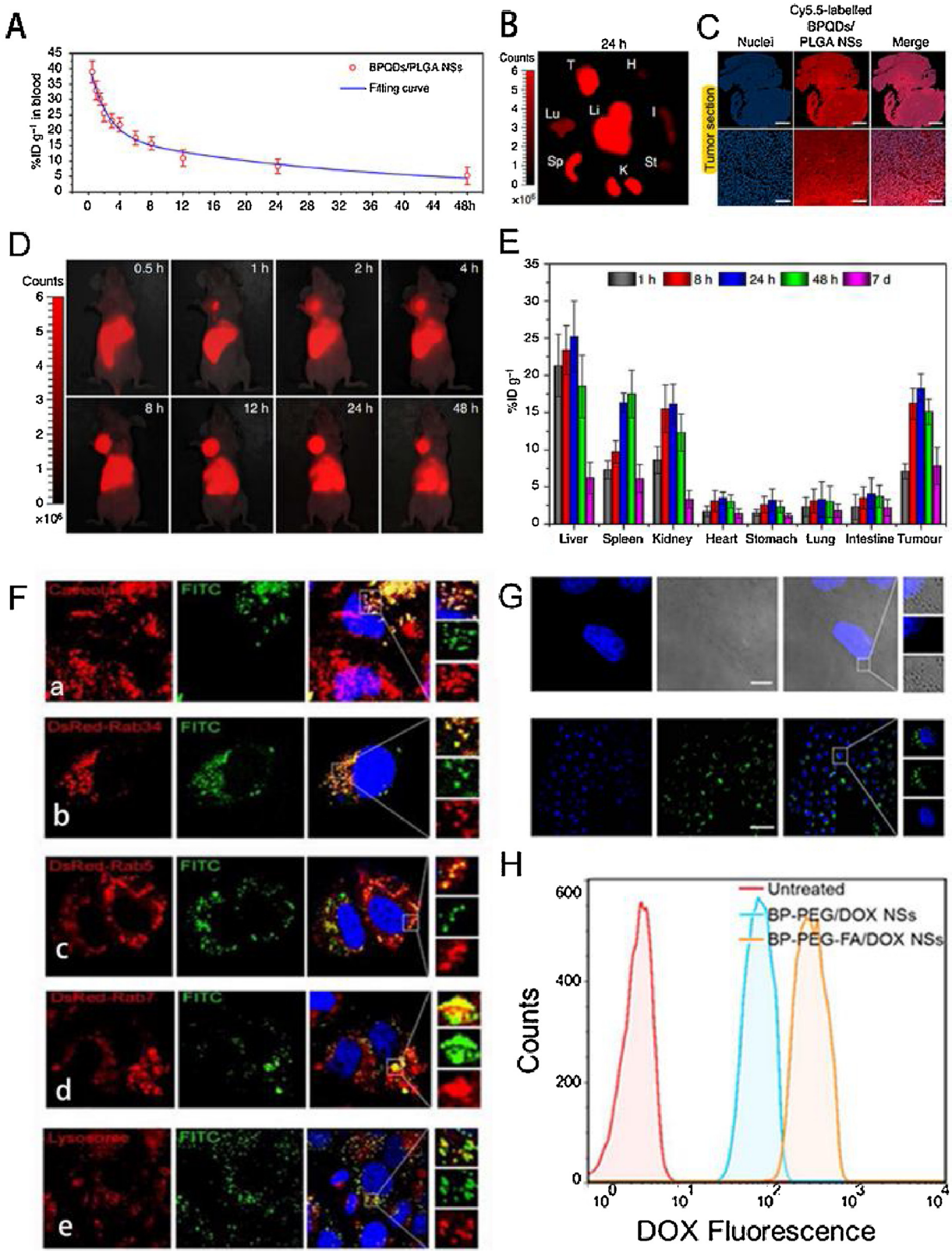

Fig. 4. Biodistribution and endocytosis pathways of BP. (A) Blood circulation curve of the Cy5.5-labelled BP NSs. (B) Fluorescence images of the tumor and major organs from the treated mice at 24 h after injection. (C) Fluorescence microscopy images of the tumor sections. (D) *In vivo* fluorescence images of the BP-treated mice. (E) Quantitative biodistribution analysis of BP in mice. Images reprinted with permission of [8] © 2016 Nature Publishing Group. (F) Endocytosis pathways of BPNSs. (G) Cellular uptake of BP-FITC NSs after 4 h-incubation with HeLa cells. (H) Flow cytometry (FCM) histogram profiles of cellular DOX fluorescence in HeLa cells at1 h after incubation with BP/DOX NSs and BP—FA/DOX NSs. Images reprinted with permission of [32]. © 2016 WILEY-VCH Verlag GmbH & Co. KGaA, Weinheim.

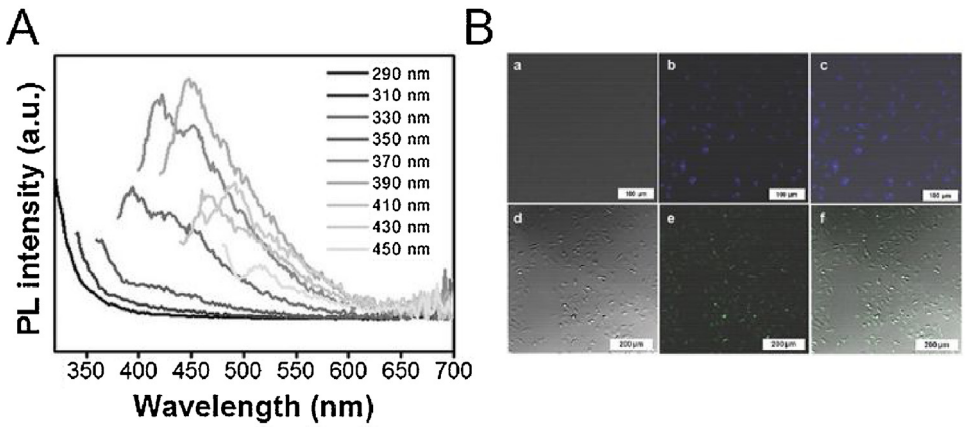

Fig. 5. (A) Fluorescence spectra of BPQDs at different excitation wavelengths. (B) Cell bioimaging of BPQDs by confocal microscopy of live HeLa cells after 12 h incubation with 1 mg/mL BPQD suspension. Images reprinted with permission of [33] © 2016 Wiley-VCH Verlag GmbH & Co. KGaA, Weinheim.

have demonstrated bright fluorescence and reduced cytotoxicity when reduced in size to below 10 nm (Fig. 5A), compared with conventional heavy metal-based QDs with long-term toxicity and environmental concerns. Furthermore, the degradation products of BP-nanodots are nontoxic intermediates. Therefore, BPQDs are becoming a potential alternative to heavy metal-based QDs because of their good biocompatibility. In 2016, H. U. Lee et al. reported the first study of BPQDs for potential biological imaging applications [33]. Fluorescent BP nanodots were fabricated by a solution exfoliation method. *In vitro* experiments demonstrated that BP nanodots can be effectively taken up by HeLa cells. Upon excitation, BP nanodots exhibited excitation wavelength-dependent fluorescence, and HeLa cells could be stained with blue and green fluorescence, indicating BP nanodots could be used for cellular fluorescence imaging (Fig. 5B). In another study, Wei Tao et al. loaded fluorescent dyes, cyanine (Cy7) and fluorescein isothiocyanate (FITC), onto PEGylated BPNS to study their *in vivo* distribution and tumor accumulation, and found that there were significant fluorescence signals especially in tumor sites [32].

Water-dispersible SiQDs provide significant advantages in QD-based optical imaging for both *in vitro* and *in vivo* studies. Tilley et al. produced water-dispersible SiQDs with blue luminescence by conjugating allylamine to the SiQDs surface [14,15]. Ruckenstein and coworkers developed poly (acrylic acid) modified SiQDs with red fluorescence for fixed cell labeling [16]. In our group, we developed acrylic acid-modified water dispersible SiQDs with yellow, green and blue photoluminescence in hydrofluoric acid solution (Fig. 6A) [17]. We recently fabricated SiQDs encapsulated in PEGylated phospholipids micelles with overall nanoconstruct diameters around 100 nm in aqueous solution. The luminescence stability of these was successfully demonstrated *in vivo* in a prostate cancer tumor model. We demonstrated *in vitro* cell labeling by confocal imaging using phospholipid-PEGylated SiQDs with pancreatic cancer cells, which paves the way for SiQDs as a potential optical probe in biomedical diagnostics (Fig. 6B). Our SiQD-based probes avoided enzymatic degradation and reticuloendothelial system (RES) capture, were stable in the acidic microenvironment of the tumor, and maintained bright and stable photoluminescence *in vivo*. SiQD-based tumor targeting, SLN mapping, and multiplex imaging were demonstrated *in vivo* with this material. Many other imaging modalities can be incorporated into SiQDs as multimodal nanoplatforms for biomedical applications. For example, optical and magnetic properties can be imparted to a single nanoplatform by combining SiQDs with iron-oxide NPs [70], manganese [93,94], or gadolinium [95].

Photothermal imaging

BP can also be used for *in vivo* thermal imaging, taking advantage of its large extinction coefficient and high PTCE at wavelengths ranging from the ultraviolet to near-infrared. Initially, C. Sun et al. simply prepared PEGylated BPNPs by a mechanical milling technique [19]. Photothermal images of mice bearing 4T1 tumors were recorded by a thermal imaging apparatus under 808 nm laser irradiation after injection of PEGylated BPNPs. The tumor temperature increased significantly from 34 °C to 59 °C within 5 min (Fig. 7A). In order to improve the BPQD stability, J. Shao et al. fabricated PLGA-coated BPQDs and measured the PTCE to be as high as 28.4% [9]. This shows promise for hyperthermia-induced tumor ablation. The tumor temperature of mice injected with the BPQDs/PLGA NSs rose rapidly by 26.3 °C within 10 min under NIR laser irradiation and the maximum temperature reached 58.8 °C (Fig. 7B). Recently, M. Qiu et al. fabricated a BP-containing hydrogel to combine localized drug delivery with a NIR-light-activated thermal agent. The photothermal effects were monitored following intratumoral injection of BP hydrogel, and the temperature changes of BP hydrogel were recorded to rise more than 13 °C compared with only 5 °C for PBS solution (Fig. 7C) [82].

Photoacoustic imaging

Photoacoustic (PA) imaging provides high spatial resolution and deep tissue penetration for visualization of physiology and pathology of tissues. In PA imaging, photons absorbed by the biological tissue or contrast agent under pulsed illumination produce a very rapid change of temperature that generates pressure transients that are detected by an acoustic transducer. PA imaging can be used for deeper tissue imaging, compared with conventional fluorescence imaging, because the light-induced acoustic waves can penetrate biological tissues more effectively. Multimodal nanoprobe-based PA imaging techniques have also been established.

Generally, both photothermal and PA effects are proportional to the absorption cross-section of the contrast agent for the incident light. Therefore, a larger absorption cross-section and higher PTCE are correlated with a more pronounced PA effect. In 2016, C. Sun et al. prepared PEGylated BPNPs as a novel PA agent for cancer diagnosis [19]. *In vitro* experiments showed that the PA imaging performance of PEGylated BPNPs increased linearly with increasing NP concentration (Fig. 8A). *In vivo* experiments showed that the tumor exhibited better signal contrast than other organs such as liver and kidney after intravenous injection of BPNPs, indicating that BPNPs accumulated mainly in the tumor

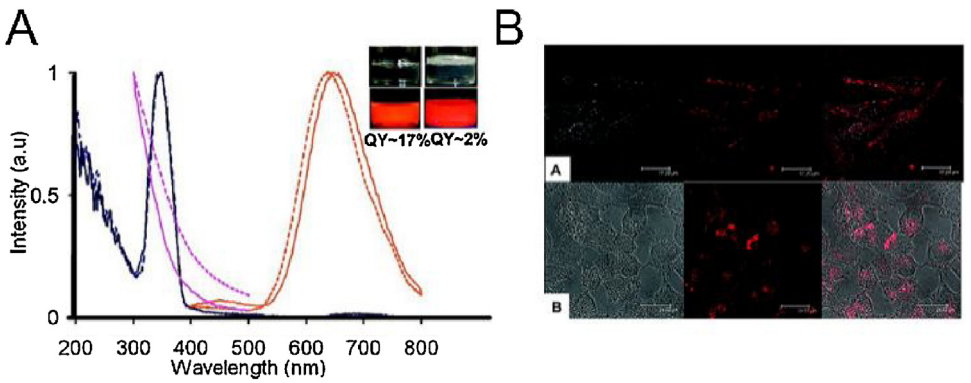

Fig. 6. (A) Optical spectra of SiQDs in chloroform and micelle-encapsulated SiQDs in aqueous solution. (B) Confocal microscopic imaging of live pancreatic cancer cells treated with amine-terminated micelle-encapsulated SiQDs and Tf-conjugated micelle-encapsulated SiQDs. Images reprinted with permission of [17] © 2008 American Chemical Society.

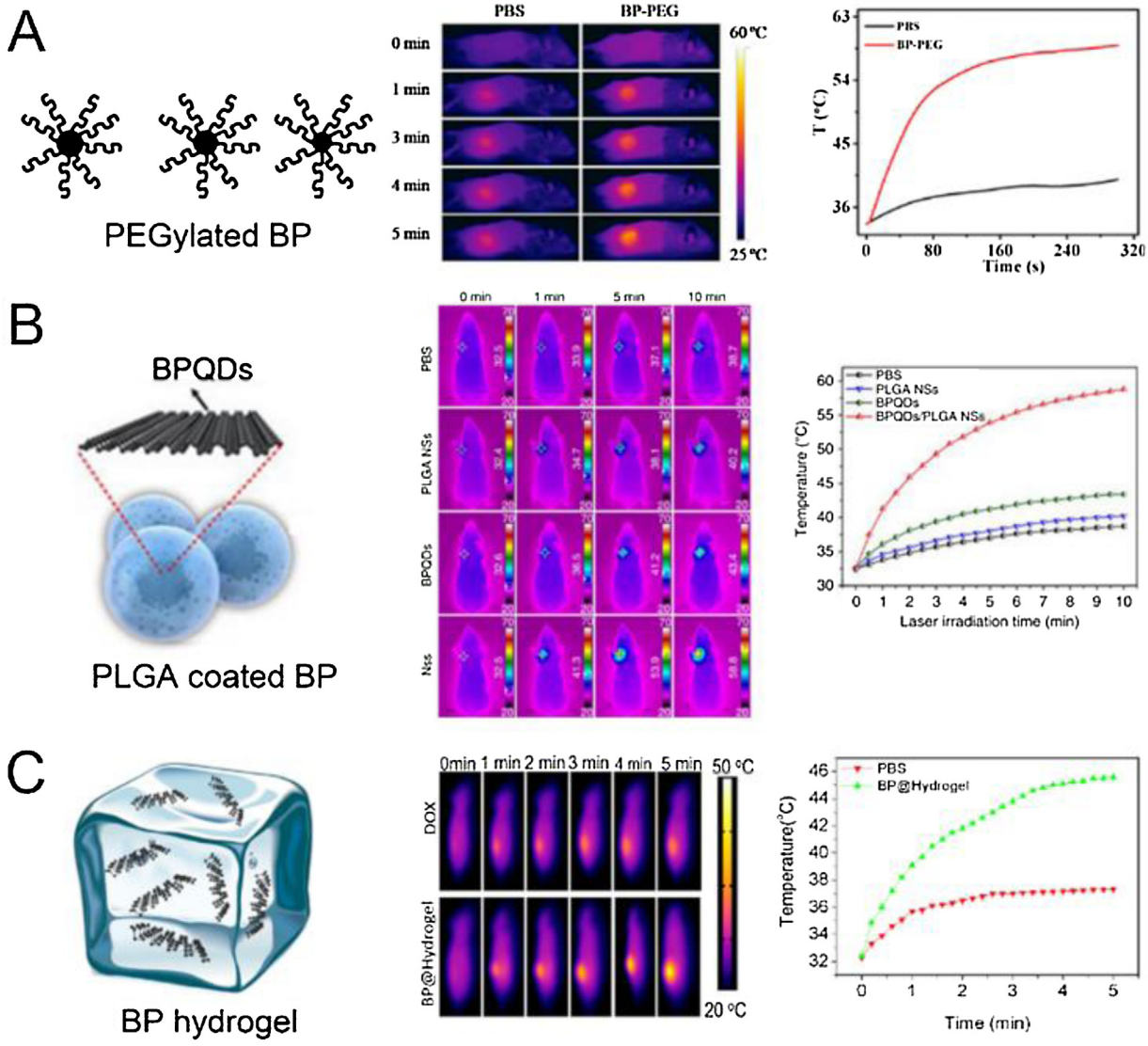

Fig. 7. NIR thermal imaging of (A) PEGylated BP. Images reprinted with permission of [19] © 2016 Elsevier B.V. (B) PLGA coated BP. Images reprinted with permission of [9] © 2015 Wiley-VCH Verlag GmbH & Co. KGaA, Weinheim. (C) BP hydrogel. Images reprinted with permission of [82] © 2018 National Academy of Sciences.

region. They concluded that PEGylated BPNPs have a longer retention time in the tumor and are cleared more rapidly from the liver and kidney (Fig. 8B). In 2017, Z. Sun et al. prepared TiL_4 coordinated BPQDs as PA agents for cancer imaging [20]. The TiL_4@BPQDs show excellent PA performance and enhanced stability in aqueous solution, compared with bare BPQDs and AuNRs. Both *in vitro* and *in vivo* experiments showed that TiL_4@BPQDs have high spatial resolution and excellent sensitivity for tumor

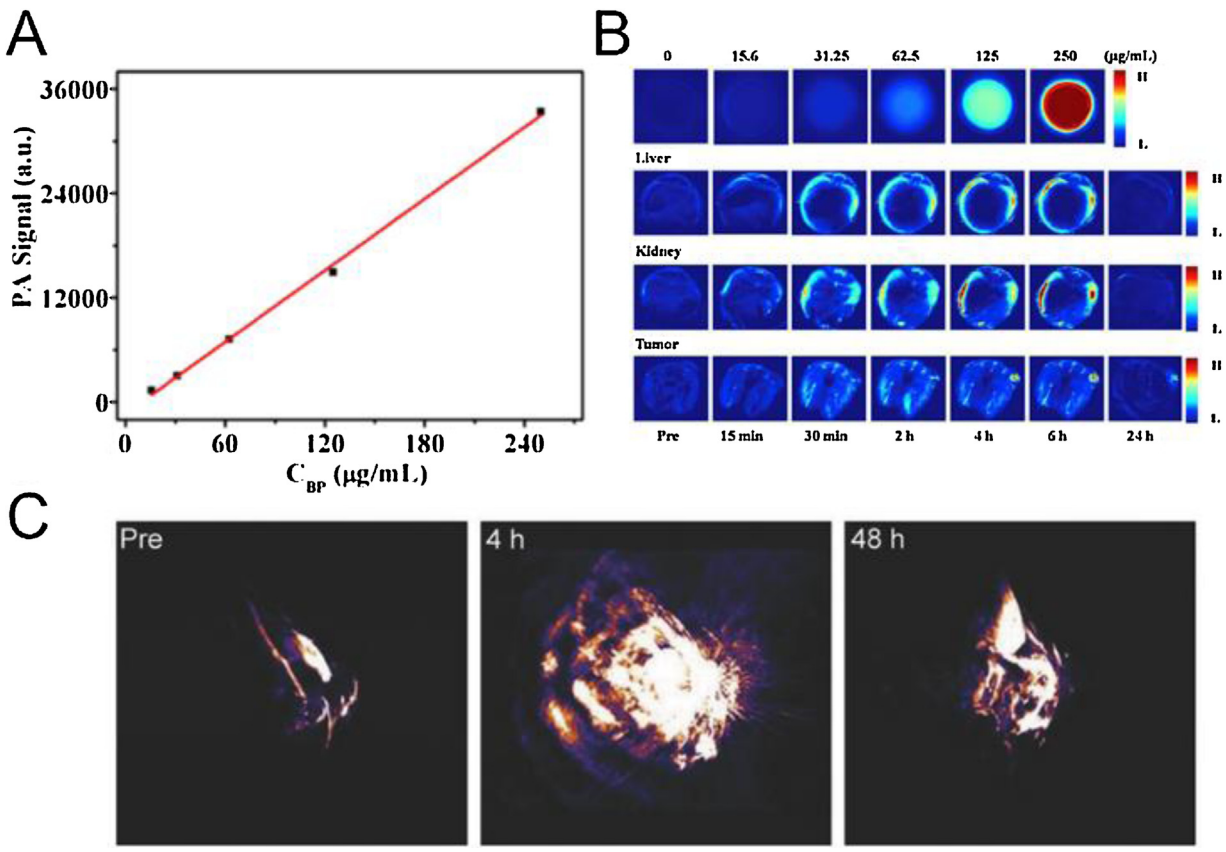

Fig. 8. (A) PA signals for different concentrations of PEGylated BPNPs. (B) *In vitro* photoacoustic images of PEGylated BPNPs solutions (first row), and *in vivo* photoacoustic images of liver, kidney, and tumor obtained at different time intervals after intravenous injection of PEGylated BPNPs, in comparison with the corresponding pre-contrast images. (C) Typical 3D PA images of the tumor at different time points pre- and post-injection of TiL_4@BPQDs. Images reprinted with permission of [20] © 2017 Wiley-VCH Verlag GmbH & Co. KGaA, Weinheim.

detection, suggesting the great potential of TiL_4@BPQDs in clinical applications (Fig. 8C).

BPNPs provide both larger extinction coefficient and higher NIR PTCE than SiNPs. Fundamentally, Si is an indirect bandgap semiconductor, which implies that SiNPs have a relatively small extinction coefficient. Thus BPNPs have been used as PA contrast agents alone, whereas nanosilicon-based contrast agents have been developed for PA imaging in combination with other contrast agents, based on porous silicon constructs. Other conventional contrast agents can be encapsulated in the rigid porous silicon nanostructure which could not only enhance the PA signal due to its low thermal conductivity but also protect the contrast agents from degradation. Zhang et al. developed silicon/carbon nanocomposites for effective PAI-guided chemo and thermal tumor treatment. These silicon/carbon NPs accumulated preferentially around tumor tissue and showed good PA signal, owing to the intrinsic large pore volume of porous silicon and NIR absorption of carbon [22]. J. Kang et al. found that the PA signal of ICG was significantly enhanced when encapsulated within rigid porous silicon, compared with free ICG or ICG within a liposomal formulation. They concluded that rigid host nanostructure with low thermal conductivity could enhance the PA signal while protecting the ICG from degradation. They demonstrated that the ICG-loaded porous silicon was an effective PA contrast agent in an *ex vivo* mouse brain model [21].

Biosensing

Early detection plays an important role in diagnosis and treatment of cancer, and the detection of serum tumor markers is one of the most common methods of tumor diagnosis. However, the concentration of tumor markers in serum is very low (pg/mL level) in the early stages of disease, so the development of highly sensitive and selective detection methods is essential for improving early diagnosis. In 2016, Yan et al. demonstrated the first few-layer BP-based non-enzymatic hydrogen peroxide (H_2O_2) sensor with a detection limit as low as of 10^{-7} M, by utilizing BP degradation under ambient conditions [96]. Kumar et al. demonstrated the first aptamer-functionalized BP-based sensing platform for the label-free detection of myoglobin (Mb), which is a cardiovascular disease biomarker [97]. This aptamer sensing platform demonstrated an ultralow detection limit of 0.524 pg mL^{-1} and sensitivity of 36 μA pg^{-1} mL cm^{-2} for Mb in serum samples. Pumera et al. demonstrated a BPNP-based label for protein detection with high selectivity. They utilized BPNPs as electrocatalytic label for the detection of rabbit immunoglobulin G (IgG) in a competitive immunoassay, by the enhanced catalytic effect of BP on the hydrogen evolution reaction (HER) [98]. They further employed BPNPs as a fluorescent sensing platform for DNA detection. A wide linear detection range as well as both low limit of detection and quantification were achieved by exploiting the affinity differences of BPNPs with fluorescence labelled single-stranded and double-stranded DNA oligonucleotides (Fig. 9A) [99]. Gu et al. developed a label-free fluorescence sensing platform for the rapid and sensitive evaluation of acetylcholinesterase (AChE) activity, by exploiting the inner filter effect (IFE) between BPQDs and 2-nitro-5-thiobenzoate anion (TNB) (Fig. 9B) [100]. The as-prepared BPQDs are photostable and acid resistant, and exhibit bright green fluorescence. Ellman's reagent (5,5′-Dithiobis-(2-nitrobenzoic acid) or DTNB), can react with thiol groups to form TNB. Based on this principle, a sensitive and label-free sensing platform was developed for fluorescence

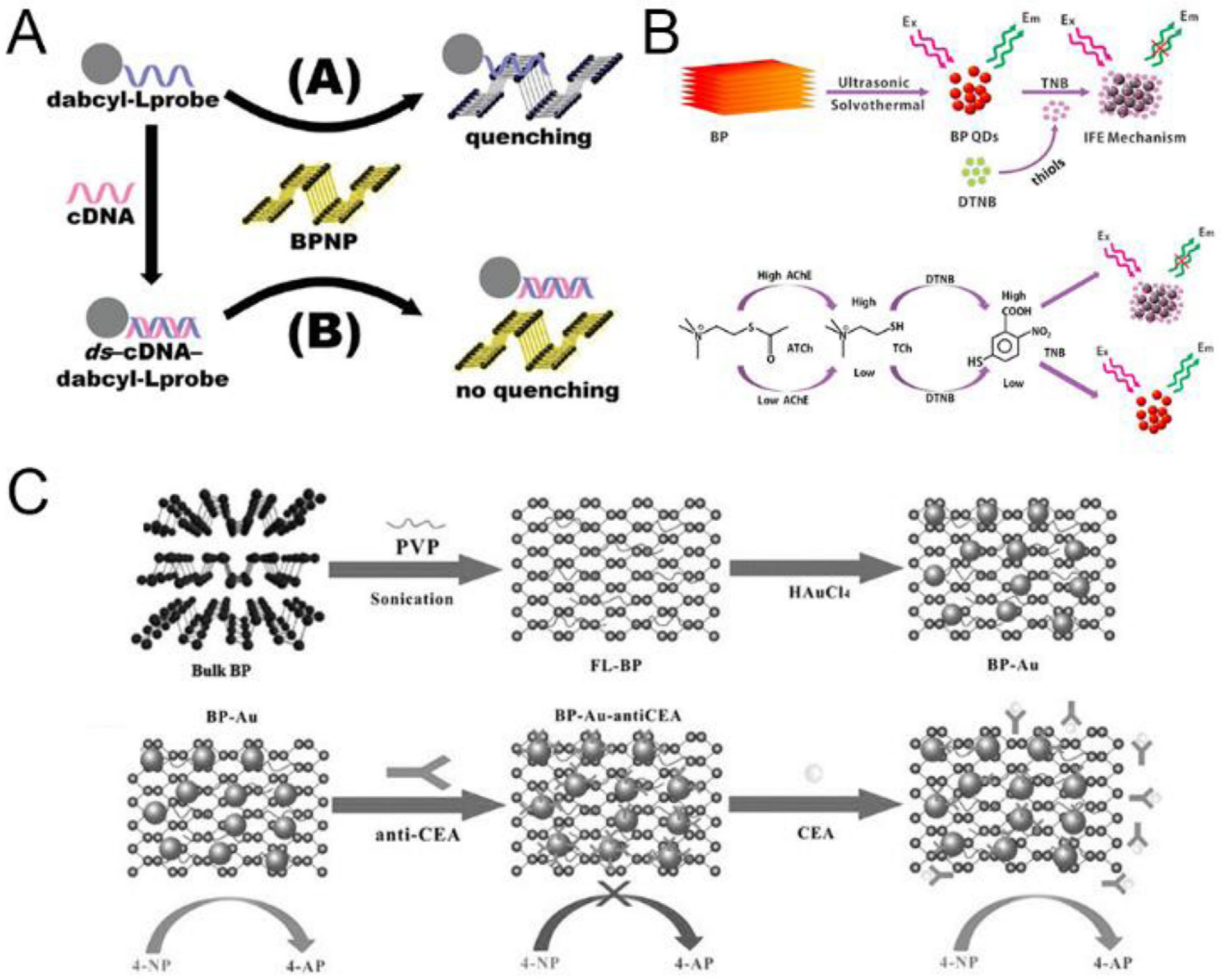

Fig. 9. (A) Schematic representation of the proposed DNA detection strategy, based on BPNPs as fluorophores. Images reprinted with permission of [100] © 2017 Elsevier B.V. (B) Schematic representation of the synthesis of BPQDs and detection of thiols and the fluorescence assay for the activity of AChE based on IFE mechanism. Images reprinted with permission of [101] © 2017 Wiley-VCH Verlag GmbH & Co. KGaA, Weinheim. (C) Schematic of colorimetric immunological detection of CEA based on the catalytic reduction 4-nitrophenol (4-NP) by BP-Au. Images reprinted with permission of [102] © Royal Society of Chemistry 2018.

measurement of thiols by virtue of the IFE between BPQDs and TNB. As a proof of concept, the platform was further used for AChE activity evaluation on acetylthiocholine substrate. Peng et al. have built a rapid and sensitive method to detect tumor markers that, for the first time, fully utilized the electronic properties of BP (Fig. 9C) [101]. They demonstrated that Au-decorated BP (BP-Au) has high catalytic activity for reduction of yellow 4-nitrophenol (4-NP) to colorless 4-aminophenol (4-AP). The catalytic activity of BP-Au is turned off with carcino-embryonic antibody (anti-CEA), due to the adsorption of anti-CEA onto the Au surface, which inhibits the catalyst activity. Thus, anti-CEA will bind with a carcinoembryonic antigen (CEA) added to form antigen–antibody complex, which desorbs the anti-CEA away from BP-Au surface, and thereby turns on the catalytic reaction. This colorimetric method for CEA detection with high sensitivity and selectivity has potential for clinical detection of CEA derived from colon and breast cancer patients. Zhou et al. developed a BPNS-based biosensing platform for rapid and sensitive microRNA detection [102]. Here, BPNSs were used as fluorescence quenchers, and the resulting BPNS-based biosensor had a linear range of 10–1000 nM, with a detection limit of 9.37 nM.

Extensive research has been done on the development of silicon-based biosensors with high sensitivity, selectivity, and multiple analyte detection ability. Cui et al. used amine, biotin and antigen functionalized nanosilicon to create field-effect transistor (FET)-based sensors for label-free and real-time detection of metal ions and proteins with high sensitivity (Fig. 10A) [103]. Patolsky et al. developed a nanosilicon-based FET, integrated with live mammalian neurons and individual axons, for simultaneous detection of the rate, amplitude, and shape of signals propagating along individual axons and dendrites [104]. Nanosilicon can also be used in a fluorescence sensor to detect biological and chemical species, due to the intense and stable fluorescence. Yi et al. demonstrated that the fluorescence of SiQDs could be quenched by H_2O_2 produced by glucose oxidase-catalyzed oxidation of glucose. This can be applied for glucose detection with high sensitivity and selectivity (Fig. 10B) [105]. Chu et al. fabricated a europium-doped nanosilicon-based ratiometric pH sensor for real-time and long-term detection of intracellular pH fluctuation in living cells [106]. To improve SERS reproducibility of free-standing metal NPs that was limited by uncontrollable size distribution and aggregation, Lee et al. prepared a series of silicon-based SERS substrates to anchor metal NPs and suppress their random aggregation [107]. The metal-decorated nanosilicon can serve as a SERS-active substrate for highly effective detection of various biological molecules (Fig. 10C).

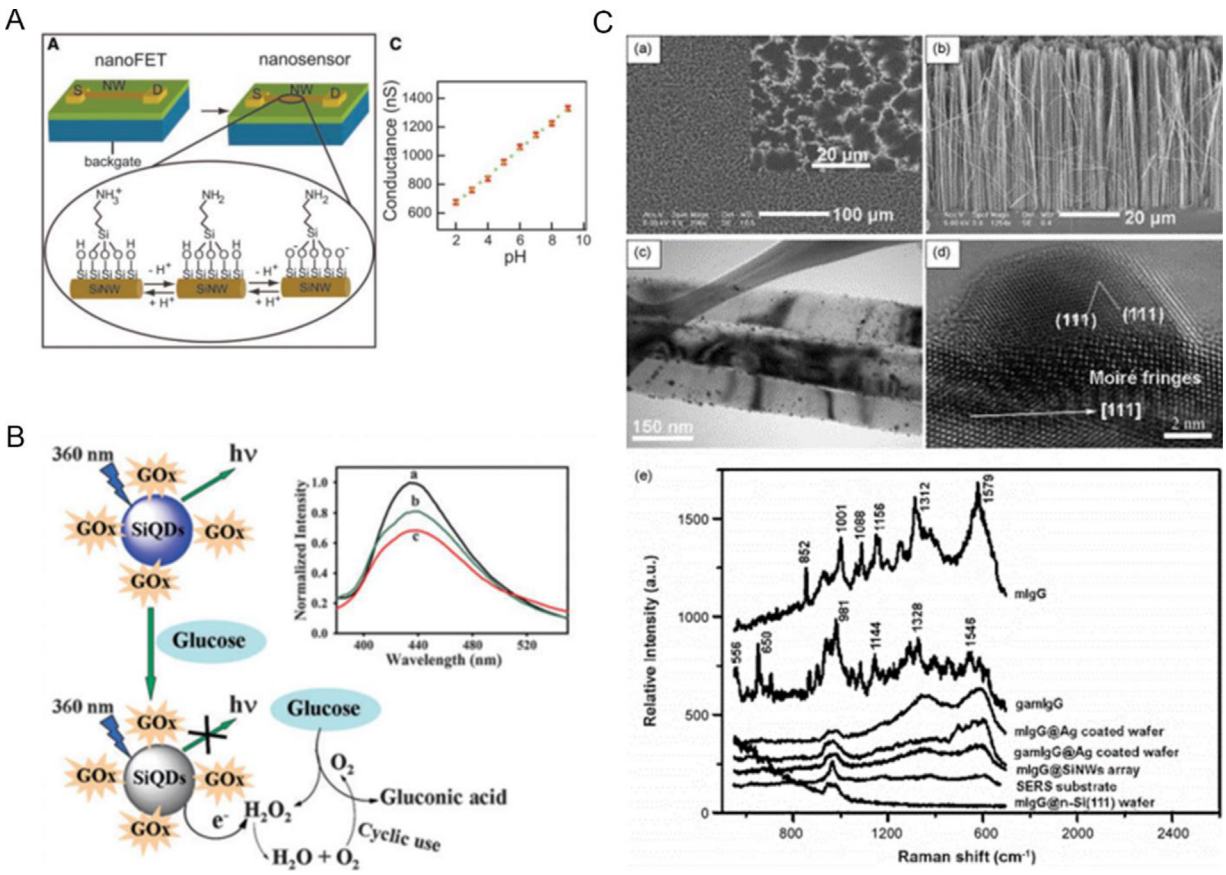

Fig. 10. (A) Schematic illustrating the conversion of a Si NW FET into NW nanosensors for pH sensing, and plot of the conductance *versus* pH. Images reprinted with permission of [103] © 2001 American Association for the Advancement of Science. (B) Schematic illustration of a glucose sensor based on H_2O_2-sensitive SiQDs. Images reprinted with permission of [105] © Royal Society of Chemistry 2013. (C) SEM and TEM mages of imetal-decorated silicon for immunoassay, and the Raman spectra of mIgG, gamIgG and their corresponding controls. Images reprinted with permission of [107] © 2010 Elsevier B.V.

Nano-therapy and drug delivery

Drug delivery

A good drug delivery system (DDS) can significantly reduce side effects and improve the efficiency of traditional chemotherapeutic agents by concentrating the drug at a target location and/or controlling the rate of drug release and activation. In the past decade, nanomaterial-based DDSs have been widely researched for the treatment of cancer and other diseases. BP nanosheets can effectively serve as a drug carrier for drug delivery, due to their 2D layered structure with ultra large specific surface area. In 2016, W. Tao et al. reported BPNSs as a robust DDS for the first time (Fig. 11A) [32]. The anticancer drug doxorubicin (DOX) could be loaded onto BPNSs with a maximum drug loading capacity of 108%, which was much higher than 10~30% typical of many NP-based delivery systems. They showed that both the NIR laser-induced hyperthermia effect of BP as well as the low pH microenvironment in the cancer cells can accelerate the drug release rate. *In vivo* assays demonstrated that PEGylated BPNSs accumulated in tumor cells through EPR effect and showed good therapeutic effect. With excellent biocompatibility and no observed cytotoxicity, DOX - loaded PEGylated BPNSs exhibited great antitumor effects both *in vitro* and *in vivo*. In another work, W. Chen et al. designed BP NSs as a DDS for DOX [108]. A high DOX loading capacity of BPNSs (950%) was achieved due to the large surface area and electrostatic interaction. The DOX release rate of BPNSs could be tuned by combined action of the acidic microenvironment and laser irradiation. *In vitro* and *in vivo* experiments demonstrated that BP NSs showed good biocompatibility and no cytotoxicity, and the tumor growth was remarkably inhibited by BP-DOX under 660 nm and 808 nm light illumination. Precision delivery of cancer drugs to the tumor site is crucial for improving therapeutic efficacy and minimizing adverse effects. M. Qiu et al. developed a new concept of applying external light with BPNPs to control drug delivery in cancer tissues (Fig. 11B) [82]. BPNSs, as photosensitizers, convert NIR light into local heating that can soften and melt anticancer drug-containing hydrogel nanostructures. Interestingly, the drug release rate can be tuned *via* several parameters, such as BP content, hydrogel composition, light intensity, and exposure time. Noticeably, optical excitation of the DOX-embedded BP hydrogel eradicated subcutaneous breast and melanoma cancers without causing any adverse effects. Moreover, this novel drug delivery system is degradable *in vivo* after treatment.

SiNPs are distinguished by their effective drug loading capacity due to their high specific surface area, approaching 500 m^2/g for 5 nm diameter NPs. Together with their good biocompatibility and facile functionalization, this allows SiNPs to be used for high-capacity drug delivery vehicles with tumor targeting ability [109]. SiNP-based nanoplatforms can facilitate the delivery of various therapeutic agents, such as small molecule drugs, proteins, and genes [55]. The *in vivo* release kinetics, biodistribution, bioavailability and side effects can be easily controlled by manipulating the size, porosity and surface chemistry of SiNPs. Due to particular physicochemical properties, SiNPs can be applied for a variety of therapeutic modalities, such as drug delivery, photothermal therapy (PTT), photodynamic therapy (PDT), radiotherapy and ultrasound diathermy for cancer treatment [29]. Bright and tumor-

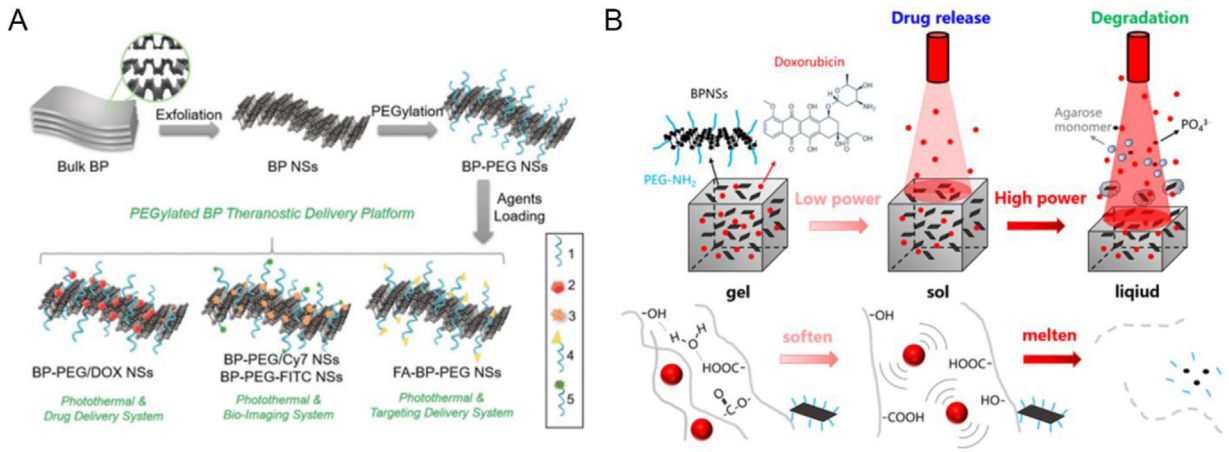

Fig. 11. (A) Schematic representation of the PEGylated BP theranostic delivery platform. Images reprinted with permission of [32] © 2016 Wiley-VCH Verlag GmbH & Co. KGaA, Weinheim. (B) Schematic illustration of the BP@Hydrogel working principle. Images reprinted with permission of [82] © 2018 National Academy of Sciences.

targeting NPs with stable fluorescence and long circulation time can be produced by micelle encapsulation and bioconjugation. Consequently, SiQDs are suitable for more sophisticated *in vivo* drug delivery [25]. Collectively, the optical properties of SiQDs make them highly suitable for diagnostics applications, for example, tumor visualization, sentinel lymph node (SLN) mapping and image guided drug delivery.

Gene delivery

Gene delivery carries genetic materials, such as RNA, DNA and oligonucleotides, into host cells to induce gene expression, inhibit undesirable gene expression, or synthesize therapeutic proteins. Ddelivery of specifically designed therapeutic genes into the appropriate cells provides a significant advancement in disease therapy [5,6]. In recent years, nonviral transfection nanovectors for gene therapy have been a very active area of investigation.

Yin et al. developed polyelectrolyte polymer-coated BPQDs to deliver electrostatically-bound LSD1 small interfering RNA (siRNA) into human ovarian teratocarcinoma PA-1 cells (Fig. 12A) [110]. LSD1 is histone demethylase, maintaining the pluripotency and proliferation of embryonic stem cells and cancer stem cells (CSCs). Thus, LSD1 has been used for targeting CSCs. The LSD1 gene targeting siRNA was delivered into PA-1 cells by loading on BPQDs. Researchers monitored the cellular uptake efficiency of siRNA/Cy3 using flow cytometry analysis (FACS) and fluorescence microscopy imaging. PA-1 cells treated with the BPQDs@PAH/siRNA nanocomplex showed the highest fluorescence signals, indicating that siRNA could be efficiently delivered to PA-1 cells by BPQDs. Compared to cells treated with PBS alone or with BPQDs@PAH, cells treated with BPQDs@PAH/siRNA showed a high rate of inhibition of LSD1 gene expression. Moreover, the key substrate of LSD1 namely mRNA level of SOX2 was down-regulated in cells treated with BPQDs@PAH/siRNA. Therefore, BPQD-based nanocomplexes showed great efficacy as a siRNA delivery platform and induced knockdown of the target gene. Finally, the investigators assessed cytotoxicity of different types of BPQDs nanocomplexes. They confirmed that the cell viability remained at 80% when the concentration of BPQDs@PAH reached 5 mg/mL, showing the good biocompatibility of these nanocomplexes. The cell growth was inhibited when treated with BPQDs@PAH/siRNA (62.1%). And the highest inhibition rate of 80% was achieved in combination with 808 nm NIR light irradiation. These results showed that BP nanocomplexes had good synergistic therapeutic effect.

Shen et al. developed a polycation-functionalized nanoporous silicon (PCPS) carrier for use as a gene silencing agent with high cargo capacity and negligible toxicity (Fig. 12B). This gene delivery system could be used to deliver siRNA and microRNA to knock down cancer gene expression in tumor bearing mice [111]. They loaded siRNA into PCPS and found that incubating MDA-MB-231 human breast cancer cells with this siRNA-loaded PCPS significantly reduced the target gene expression *in vitro*. In a MDA-MB-231 breast cancer bearing murine model, the siRNA-loaded PCPS accumulated in tumor tissues after systemic delivery, reduced the expression of the target gene in cancer cells, and significantly reduced cancer stem cells in the residual tumor tissue. They further demonstrated that the siRNA-loaded PCPS did not trigger acute immune response in FVB mice at the therapeutic dosage.

Photothermal therapy (PTT)

PTT has drawn much attention and been extensively explored, due to its minimal invasiveness and high therapeutic efficiency. PTT can effectively ablate cancerous cells by disrupting the cell membrane or microenvironment through highly localized heating. This rapid local heating is achieved using a light-absorbing agent as a photosensitizer to absorb photons and dissipate their energy as heat. PTT ablative therapies are based on a physical heating mechanism, and can therefore be applied for chemotherapy-resistant cancer treatment, and can promote increased tumor response in combination with chemotherapy and radiation.

BPNSs and BPQDs display broad absorption across the entire visible and NIR spectral ranges. Thus, BP has NIR photothermal properties that can be applied for photothermal treatment. In 2015, Z. Sun et al. fabricated BPQDs by a controllable liquid exfoliation method that combined probe sonication and bath sonication methods [9]. The ultra-small BPQDs showed a large extinction coefficient of 14.8 L g^{-1} cm^{-1} at 808 nm and an excellent NIR PTCE of 28.4%. Under NIR irradiation, the BPQDs produced substantial killing of C6 and MCF7 cancer cells, demonstrating the great potential of BPQDs as PTT agents. To further improve the biostability of BP under physiological conditions, J. Shao et al. developed biodegradable BPQD/PLGA NPs with diameter around 100 nm (Fig. 13A) and enhanced stability for several weeks (Fig. 13B-D) [8]. Their *in vitro* and *in vivo* experiments demonstrated that the BPQD/PLGA NPs have negligible intrinsic cytotoxicity and good biocompatibility (the degradation process is illustrated in Fig. 13E), combined with excellent PTT efficiency and tumor targeting ability to ablate tumors under NIR irradiation.

The ability of radio frequency (RF) radiation to heat tissues, leading to effective necrosis of tumors, is well known and has shown promise for clinical translation. Properly designed sensi-

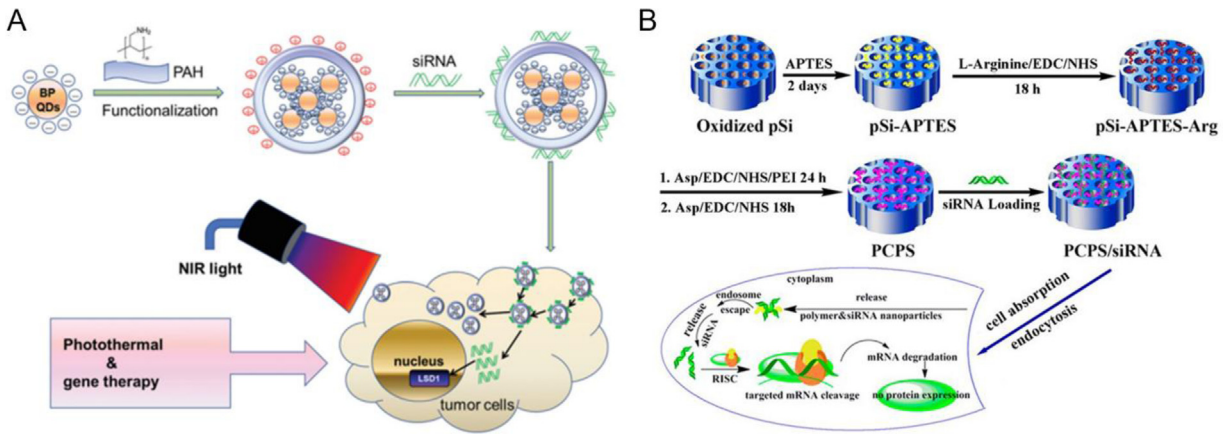

Fig. 12. Schematic illustration of (A) BPQDs@PAH siRNA therapeutic mechanism. Images reprinted with permission of [110] © Royal Society of Chemistry 2017. (B) Fabrication of PCPS as a delivery carrier for gene silencing agents. Images reprinted with permission of [111] © 2013 American Chemical Society.

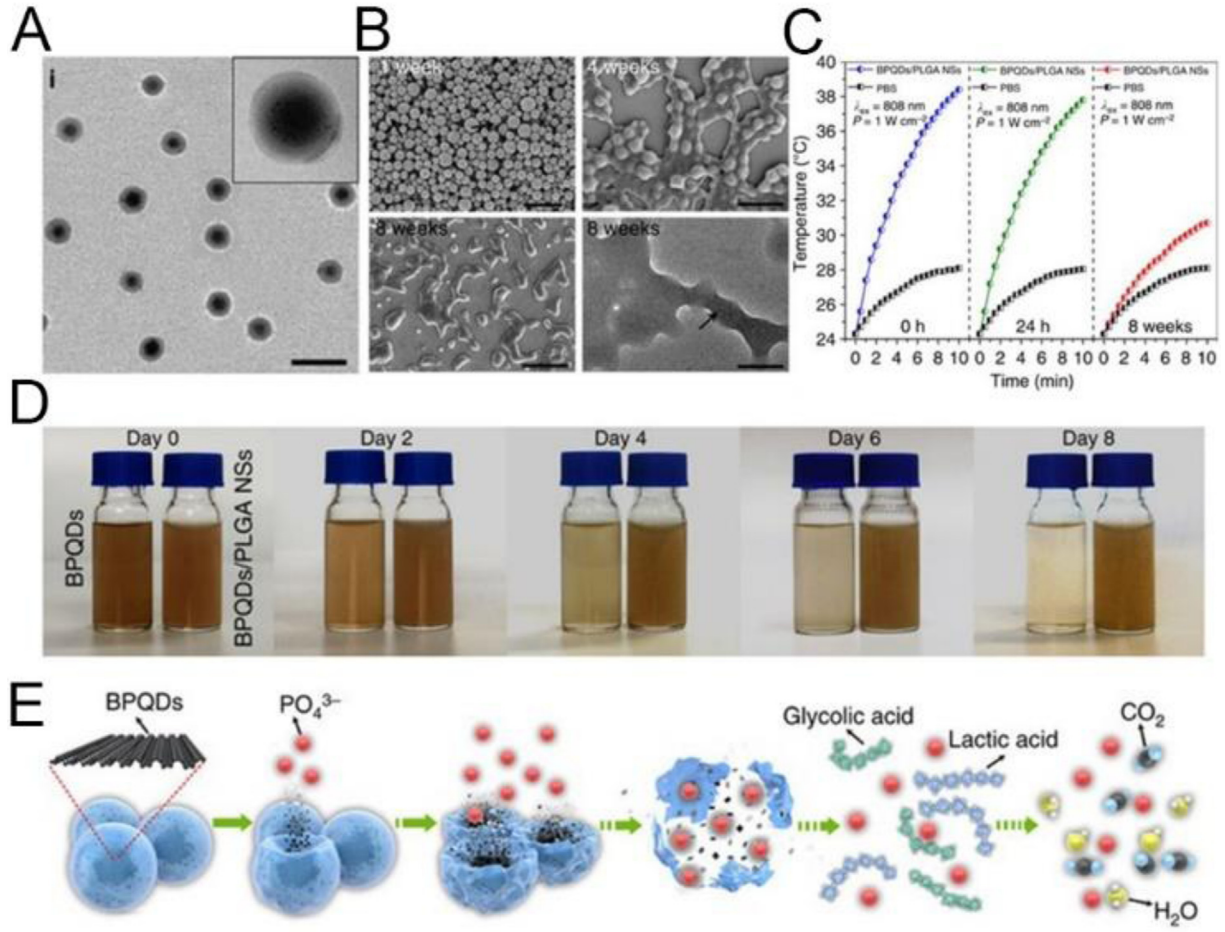

Fig. 13. (A) TEM and (B) SEM images of the BPQD/PLGA NSs. (C) Photothermal heating curves of the BPQD/PLGA NSs dispersed in PBS for 0 h, 24 h and 8 weeks and irradiated with an 808 nm laser. (D) Photographs of the BPQDs and BPQDs/PLGA NSs in water after different periods of time. (E) Schematic representation of the degradation process of the BPQD/PLGA NSs in the physiological environment. Images reprinted with permission of [8] © 2016 Nature Publishing Group.

tizers with tumor targeting ability can significantly enhance the efficacy of RF-based therapy by absorbing RF radiation energy to generate hyperthermia that leads to selective destruction of cancer cells. Tamarov et al. developed a SiNP-based sensitizer of RF radiation to generate hyperthermia for cancer treatment (Fig. 14) [7]. Both by mechanical grinding of porous silicon and by ultraclean laser-ablative synthesis, they developed SiNPs that can effectively generate RF-induced heating to temperatures above 45̄0 °C at clinically achievable concentrations (1 mg/mL). *In vivo* experiments demonstrated that low intensity RF radiation excitation of SiNPs can strongly inhibit the growth of carcinoma tumors, and even decrease the tumor volume.

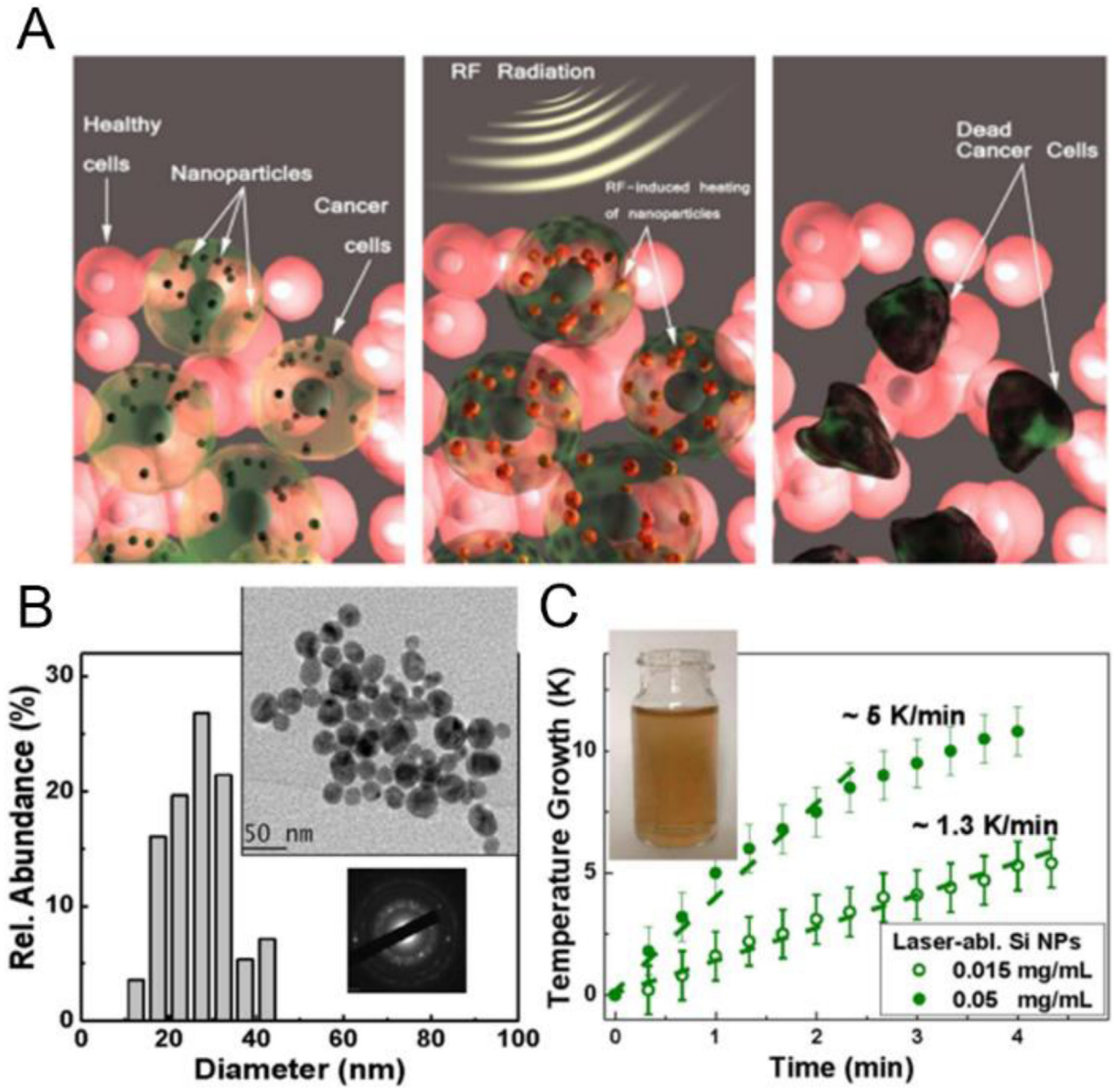

Fig. 14. (A) RF radiation-induced hyperthermia using RF-absorbing Si nanoparticle-based sensitizers. (B) TEM image (inset), electron diffraction pattern (inset) and corresponding size distribution of NPs prepared by laser ablation from a Si target in deionized water. (C) Temperature increase of an aqueous suspension of laser-ablated Si-based NPs at a concentration of 0.015 mg/mL. Images reprinted with permission of [7] © 2018 Springer Nature Limited.

Photodynamic therapy (PDT)

Hyperthermia triggered by PTT can potentially cause inflammatory disease as well as damage to other nearby organs. PDT is another form of phototherapy in which a photosensitizing agent is activate by light and then transfers its energy to oxygen molecules to produce reactive singlet oxygen ($^1O_2$) species, leading to the necrosis of cancerous cells. Many photosensitizers (PS), including organic molecules, heavy-atom-containing compounds, and noble metals can produce $^1O_2$ *in vivo* under light irradiation. However, their further applications have been limited by low quantum yield, easy photobleaching, or poor water solubility. Therefore, novel photosensitizers with high $^1O_2$ quantum yield and good biocompatibility are still urgently needed.

In 2015, Wang *et al.* first demonstrated that BPNSs can be used as a photosensitizer for high efficiency generation of $^1O_2$, which can be applied for PDT (Fig. 15A). BPNSs can generate $^1O_2$ across the whole visible spectrum, with a quantum yield as high as 0.91 [10]. Both *in vitro* and *in vivo* experiments indicated that BPNSs with good aqueous dispersibility show excellent anticancer effects. In addition, the ability of BPNSs to degrade to biocompatible phosphorus oxides further highlights their potential for clinical translation against cancer. However, as-prepared BP can only respond to visible light for PDT, which severely limits tissue-penetration. To solve this problem, Lv *et al.* fabricated a multifunctional nanocomposite by loading upconversion NPs (UCNPs), that served as an energy donor, onto BPNSs *via* electrostatic interaction, creating a NIR light-mediated PDT agent (Fig. 15B) [11]. The UCNP component upconverts 808 nm illumination to a shorter wavelength that is absorbed by the BPNS to generate ROS, as demonstrated by both *in vitro* and *in vivo* experiments. In 2017, Yang et al. developed a novel BP@Au@Fe_3O_4 nanocomposite by assembly of Fe_3O_4 NPs and Au NPs onto BPNSs (Fig. 15C). This nanocomposite structure exhibits a wide spectrum absorption and was also photodegradable, to allow clearance of its components [18]. The resulting magnetic resonance imaging (MRI)-guided synergistic

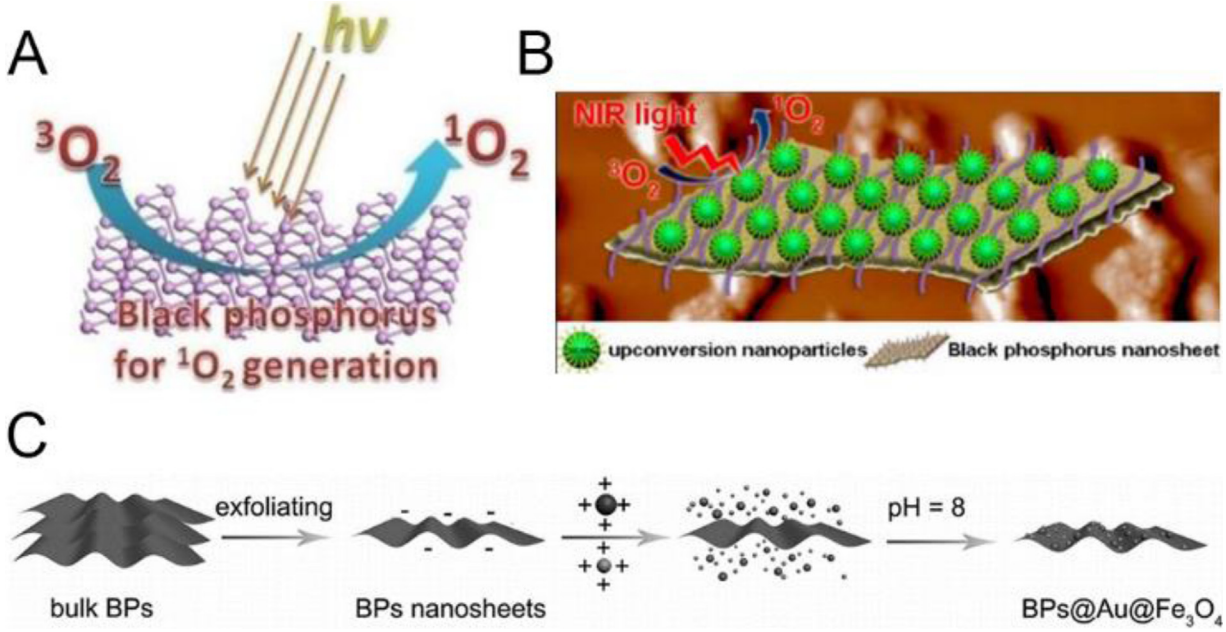

Fig. 15. (A) Schematic illustration of ROS generation by BPNSs under irradiation. Images reprinted with permission of [10] © 2015 American Chemical Society. (B) Schematic illustration of ROS generation by UCNP loaded-BPNSs under NIR irradiation. Images reprinted with permission of [11] © 2016 American Chemical Society. (C) Schematic illustration of the fabrication of BP@Au@Fe_3O_4 nanoplatform. Images reprinted with permission of [18] © 2017 Wiley-VCH Verlag GmbH & Co. KGaA, Weinheim.

photothermal and photodynamic tumor inhibition efficacy was demonstrated by both *in vitro* and *in vivo* experiments.

The tunable luminescence characteristics and $^1O_2$ generation ability of SiNPs under excitation of visible and NIR irradiation also make SiNPs good candidates for PDT applications. Rioux et al. prepared SiNPs by laser ablation in liquids and showed that they could act as photosensitizers to produce $^1O_2$ and kill microbes. [12] The colloidal SiNPs with well-defined size were fabricated by femtosecond laser ablation. The SiNPs can generate $^1O_2$ upon laser irradiation over a wide spectral range without being photobleached, suggesting their potential as photosensitizers for therapeutic application.

Neurodegenerative disorder therapy

The blood-brain barrier (BBB) is a major obstacle for treatment of neurodegenerative disorders (NDs), including Parkinson's disease and Alzheimer's disease. The BBB, which is made up of astrocyte-enclosed brain capillary endothelial cells, is an important physiological barrier in the central nervous system. It regulates the transport of molecules from the circulatory system into the brain. Delivery of diagnostic and therapeutic agents across the BBB to treat NDs is still a major challenge. The BBB regulates the selective and specific transport of exogenous and endogenous molecules to the brain. Only liposoluble molecules, alcohol, anesthetics and some low molecular mass compounds can pass through the capillary walls. Various factors, including the surrounding surfactants, NP size, and electric charge determine whether NPs can cross the BBB successfully. Recently, the interface between nanomaterials and neuroscience has opened the door for appealing new therapeutic strategies. Chen et al. demonstrated that BPNSs can have enhanced BBB permeability under near-infrared (NIR) irradiation, due to their photothermal effect [112]. Moreover, the ability of phosphorus to bind specific metal ions makes BP a robust nanocaptor for Cu^{2+}, which plays a crucial role in the etiology of NDs, suggesting that BP can be a new neuroprotective platform for ND treatment, in addition to triggering transcytosis through the BBB (Fig. 16). Chen et al. first investigated the ability of BPNSs to improve BBB permeability using an *in vitro* BBB model made up of a monolayer of bEnd.3 cells. They found that transport of BPNSs across the monolayer was significantly enhanced under NIR irradiation, suggesting improved BBB permeability due to the photothermal effect of BPNSs. *In vitro* cell viability testing indicated that almost all the cells were dead when cultured with Cu^{2+} and ascorbic acid (AA), implying that the elevated intracellular ROS concentration significantly decreased the cell viability of SH-SY5Y. In contrast, cell viability was recovered when BP nanosheets were added along with Cu^{2+} and AA, indicating BP nanosheets can protect SH-SY5Y cells from Cu^{2+} dyshomeostasis and oxidative stress-induced cell apoptosis. Furthermore, they investigated the ability of BPNSs to cross the BBB *in vivo*. One hour after intravenous injection of BPNSs, the head temperature was increased to 42.2 °C under NIR irradiation, as indicated in Figure 18b. Both the observation of staining with Evans blue and NIR fluorescence imaging showed that transport across the BBB was improved by the photothermal effect of laser heated BP nanosheets.

Combination and synergistic therapy

Monotherapy is well known to suffer from poor therapeutic effect, due to drug resistance, diversity of cancer, and personal specificity of patients, leading to poor curative effect and lack of complete cure. In contrast, combination treatments of cancers have drawn research interest owing to their unique advantages including low side effects and high therapeutic efficacy. On the other hand, developing multi-functional systems for combination therapy often requires complex design and synthesis procedures, which can make it impractical for clinical applications. Recently, great progress in SiNP and BPNP technologies has brought new hopes for combination therapy. The aforementioned distinguishing properties make SiNPs and BPNPs highly promising nanoplatforms for multidisciplinary biomedical applications. BP has excellent photophysical properties that can generate $^1O_2$ and hyperthermia for PDT and PTT. In addition, because of the puckered layered structure and relatively large surface area, BP can serve as an efficient vehicle for delivering various agents. Therefore, BPs can be utilized as plat-

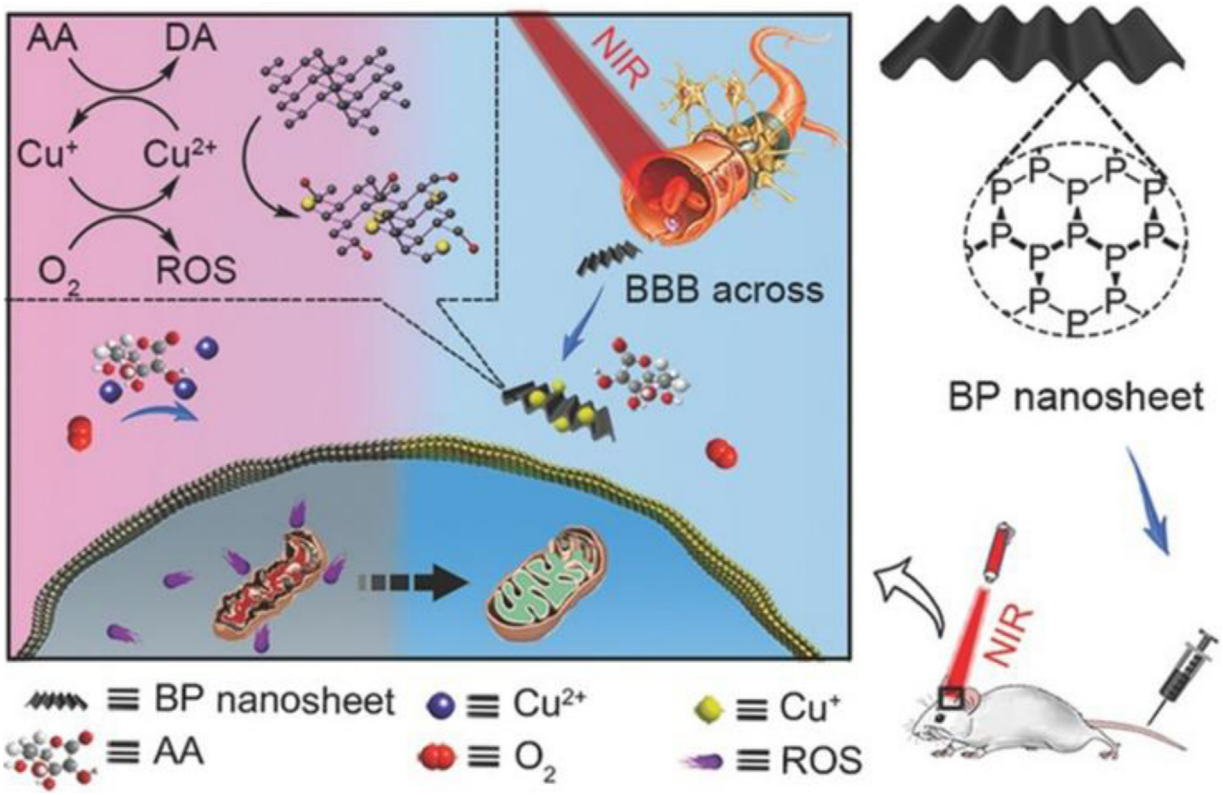

Fig. 16. Schematic illustration of BP nanosheets as a BBB penetrating nanocaptor to decrease the oxidative stress production by capturing Cu ions for ND therapy. Images reprinted with permission of [112] © 2018 Wiley-VCH Verlag GmbH & Co. KGaA, Weinheim.

forms for combination therapy. Yang *et al.* combined iron oxide NPs and Au NPs on BPNSs [18]. They demonstrated combined action of photodynamic and photothermal effects by BPNSs and plasmonic photothermal effect from Au NPs, together with MRI contrast enhancement from Fe_3O_4 NPs. Chen *et al.* designed a BPNS-based multimodal therapeutic system for cancer treatment by exploiting the ultrahigh drug loading capacity and excellent photophysical properties of BP. [108] *In vitro* and *in vivo* experiments demonstrated that BP-DOX showed synergistic PDT/PTT/chemo therapy and remarkable inhibition of tumor growth under 660 and 808 nm light. A same type of strategy has also been used with silicon nanowires. Guo *et al.* fabricated a multifunctional silicon-based system by decorating silicon nanowires with iron oxide and Au NPs [113]. This system could load therapeutic drug with high drug loading capacity and be simultaneously responsive to pH changes, NIR light, and magnetic fields, enabling highly efficient synergistic treatment of drug-resistant cancer.

Theranostics

Theranostics, which combine imaging or diagnostic functions with therapeutic function, allow disease diagnosis and therapy, as well as simultaneous imaging-guided therapy. FLBP is an ideal theranostic material that has intrinsic fluorescence and PA contrast for imaging as well as PTT and PDT properties for therapy [19,114]. Furthermore, FLBP can be easily endowed with multiple, diverse functionalities by surface modification or cargo loading through a few synthetic steps. Fluorophores can be linked to or loaded onto the surface of FLBP to perform *in vitro* or *in vivo* fluorescence imaging. AuNPs can enhance the PTT efficacy of the whole system and endow the system with the potential to perform Raman bio-detection *via* SERS [115]. In addition, introducing iron oxide NPs onto FLBP can allow visualization of nanoparticle distribution *via* MRI [18]. Imaging data allow the bioactivities of FLBP-based nanosystems, such as transport pathways and cellular localization, to be understood, and the data contribute to pinpointing the tumor region for precise obliteration of malignant cells with reduced side effects. Erogbogbo et al. integrated biomarker discovery techniques into rationally-designed SiNPs to improve the disease-specific diagnosis and treatment [30]. Therefore, SiNPs and BPNPs-based diagnosis-guided therapy shows great potential in the biomedical field.

Summary and perspectives

In conclusion, this present review comprehensively summarized recent progress in SiNPs and BPNPs research, including preparation methods, fundamental properties, and biomedical applications. In the past few years, substantial effort has been devoted to the fabrication and biomedical applications of BP-based nanomaterials, whereas the history of biomedical applications of SiNPs is somewhat longer. SiNPs and BPNPs are both inorganic nanomaterials with intrinsic advantages including abundance, biocompatibility, and low cost. When one or more of their dimensions are reduced to the nanoscale, these materials develop photophysical features that make them, in some ways, superior to heavy metal-based nanomaterials for biomedical applications. Nevertheless, there are some significant differences between the two nanomaterials arising from of the fundamental dissimilarities of SiNPs and BPNPs. The most widely researched silicon nanostructures for biomedical applications are porous silicon particles and SiQDs, both of which generally require multistep fabrication processes. The lack of convenient preparation processes like those used for gold NPs or cadmium-based quantum dots has somewhat slowed the development of SiQDs in biomedical applications. In contrast to the complex fabrication requirements for SiNPs, few-

layer BP can be prepared by liquid phase exfoliation method, taking advantage of the very weak interlayer interactions in BPNSs, arising only from van der Waals forces. The liquid phase exfoliation method is comparatively a simpler process and less expensive, and is very advantageous for scale-up production and bio-applications of the few-layer 2D BPNPs.

Toxicity of nanomaterials is difficult to assess without considering their synthetic origin, surface functionalization, size, and cell type or experimental animal used. In the *in vitro* cytotoxicity assessment to date, both SiNPs and BPNPs have shown minimal toxicity, and both can be degraded to harmless products. However, SiNPs have the subject of more *in vivo* studies, including a study in primates. The toxicity assessment of BPNPs to date extends only to mice and includes far fewer studies than for SiNPs. Thus, further systematic and long-term biosafety evaluation of BPNPs must still be conducted, but all indications are that BPNPs will be biocompatible at doses useful for imaging and therapy.

Because of their longer history of development, studies of imaging using SiNPs are more numerous and advanced than those using BPNPs. Various SiQDs with good photo-stability and potential for multicolor imaging have been developed. SiQDs with photoluminescence at wavelengths from blue to the NIR can provide significant advantages in QD-based optical imaging and hold great promise as valuable optical probes in biomedical diagnostics. Compared with the extensive related research on nanosilicon, bio-imaging studies conducted using BPNPs photoluminescence are less numerous. BPNPs are increasingly being studied for photoacoustic and photothermal imaging under NIR laser irradiation. These methods greatly enhance tissue penetration depth and reduce the risk of phototoxicity.

With respect to drug delivery, SiNPs have been demonstrated to enhance delivery of various drugs in various studies showing that nanoporous silicon could carry up to 80% loading of drugs. As compared with silicon, a higher drug loading capacity of 950% was achieved with 2D BPNSs due to its exceptionally large surface area. Methods of loading the drug onto the two kinds of nanostructures structure are different. Covalent attachment, physical trapping by oxidation and spontaneous adsorption were utilized in the loading process of nanoporous silicon while 2D BPNSs were coated with the polymers and drugs through electrostatic interactions. The nanoporous silicon could deliver more variety of drugs than the 2D BPNSs. The regular spherical shape of nanoporous silicon also facilitated delivery and transmembrane diffusion *in vivo*. Thus, besides taking drug loading capacity into account, the diversity of drugs that can be loaded and the delivery efficiency should also be subjects of further studies of 2D BPNSs.

In the field of cancer treatment, BPNPs were mainly developed as efficient photothermal conversion agents for PTT, while Si nanostructures have been used as sensitizers of PDT as well as for RF radiation-induced hyperthermia. RF radiation can penetrate deeper into the body than NIR laser irradiation for PTT, which will benefit therapy of deep tumors. On the other hand, BPNSs display broader and stronger absorbance across the whole visible spectrum. The ultra-small BPNPs exhibited large extinction coefficient and high photothermal conversion efficiency. As a result, the dosage of BP for PTT is significantly lower than the Si for RF treatment to achieve sufficient heating to inhibit the growth of cancer cells. This lower dose could significantly reduce the potential for unwanted side-effects.

BPNPs have become a research hotspot in the recent years, while research on SiNPs has begun earlier, proceeded more slowly, and made some outstanding achievements over the past decade. Nevertheless, the differences and the weaknesses of both nanomaterials that may influence the biomedical applications must still be further studied, before they advance from the laboratory to the clinic.

Up to now, nearly all studies of the biomedical applications of nanosilicon and BP are confined to cancer therapy. Other biofunctions of SiNPs and BPNPs can potentially be employed in many other multidisciplinary biomedical applications, such as antibacterial therapy, tissue engineering and progressive brain disease [116]. Finally, so far, all the silicon and BP based biomedical applications have been demonstrated in the laboratory, mainly with *in vitro* and some small animal *in vivo* experiments. Substantial additional preclinical studies are still required before the successful clinical translation. The diversity of preparation methods employed for SiNPs and BPNPs my complicate the pathway to the clinic, because pre-clinical testing of materials prepared by one method may not be accepted as a demonstration of safety or efficacy of materials prepared by another method. Because different methods produce materials that are optimal for different applications, multiple forms of SiNPs and BPNPs may have to proceed through regulatory approval processes independently. Moreover, the methods for preparing and characterizing these and other inorganic nanomaterials are often unfamiliar to regulators, and thus these materials may be treated with greater caution than more conventional drugs.

There is no doubt that their further clinical translation will require the participation of researchers from a variety of disciplines including nanoscience, pharmacy, medicine, and engineering. Consequently, the continuous development of silicon and BP nanotechnology will provide limitless applications in various biochemical and medical areas, and more basic research and technological breakthroughs will be achieved in the near future.

Acknowledgements

This study was supported by the National Natural Science Foundation of China (NSFC) (61435010 and 61875138); The Science and Technology Innovation Commission of Shenzhen (JCYJ20170818093453105); The China Postdoctoral Science Foundation (2017M610540, 2018T110892); The PhD Start-up Fund of Natural Science Foundation of Guangdong Province, China (2018A030310500); The PhD Fund of Natural Science Foundation of Shandong Province, China (ZR2016BB33). PNP acknowledges support from the MEPhI Academic Excellence Project (Contract No. 02.a03.21.0005). This paper is dedicated to our co-author, Dr. Ajay Singh, who unexpectedly passed away on October 20, 2018.

References

[1] K. Yong, W. Law, R. Hu, L. Ye, L. Liu, M.T. Swihart, P.N. Prasad, Chem. Soc. Rev. 42 (2013) 1236–1250.
[2] G. Chen, H. Qju, P.N. Prasad, X. Chen, Chem. Rev. 114 (2014) 5161–5214.
[3] G. Chen, I. Roy, C. Yang, P.N. Prasad, Chem. Rev. 116 (2016) 2826–2885.
[4] G. Xu, S. Zeng, B. Zhang, M.T. Swihart, K. Yong, P.N. Prasad, Chem. Rev. 116 (2016) 12234–12327.
[5] P.N. Prasad, Introduction to Biophotonics, John Wiley & Sons, 2004.
[6] P.N. Prasad, Nanophotonics, John Wiley & Sons, 2004.
[7] K.P. Tamarov, L.A. Osminkina, S.V. Zinovyev, K.A. Maximova, J.V. Kargina, M.B. Gongalsky, Y. Ryabchikov, A. Al-Kattan, A.P. Sviridov, M. Sentis, A.V. Ivanov, V.N. Nikiforov, A.V. Kabashin, V.Y. Timoshenko, Sci Rep-Uk 4 (2014) 7034.
[8] J. Shao, H. Xie, H. Huang, Z. Li, Z. Sun, Y. Xu, Q. Xiao, X. Yu, Y. Zhao, H. Zhang, H. Wang, P.K. Chu, Nat. Commun. 7 (2016) 12967.
[9] Z. Sun, H. Xie, S. Tang, X. Yu, Z. Guo, J. Shao, H. Zhang, H. Huang, H. Wang, P.K. Chu, Angew. Chemie Int. Ed. English 54 (2015) 11526–11530.
[10] H. Wang, X. Yang, W. Shao, S. Chen, J. Xie, X. Zhang, J. Wang, Y. Xie, J. Am. Chem. Soc. 137 (2015) 11376–11382.
[11] R. Lv, D. Yang, P. Yang, J. Xu, F. He, S. Gai, C. Li, Y. Dai, G. Yang, J. Lin, Chem. Mater. 28 (2016) 4724–4734.
[12] D. Rioux, M. Laferriere, A. Douplik, D. Shah, L. Lilge, A.V. Kabashin, M.M. Meunier, J. Biomed. Opt. 14 (2009) 021010.
[13] H.U. Lee, S.Y. Park, S.C. Lee, S. Choi, S. Seo, H. Kim, J. Won, K. Choi, K.S. Kang, H.G. Park, H. Kim, H.R. An, K. Jeong, Y. Lee, J. Lee, Small 12 (2016) 214–219.
[14] R.D. Tilley, K. Yamamoto, Adv. Mater. 18 (2006) 2053–2056.
[15] J.H. Warner, A. Hoshino, K. Yamamoto, R.D. Tilley, Angew. Chemie Int. Ed. English 44 (2005) 4550–4554.
[16] Z.F. Li, E. Ruckenstein, Nano Lett. 4 (2004) 1463–1467.

[17] F. Erogbogbo, K. Yong, I. Roy, G. Xu, P.N. Prasad, M.T. Swihart, ACS Nano 2 (2008) 873–878.
[18] D. Yang, G. Yang, P. Yang, R. Lv, S. Gai, C. Li, F. He, J. Lin, Adv. Funct. Mater. 27 (2017) 1700371.
[19] C. Sun, L. Wen, J. Zeng, Y. Wang, Q. Sun, L. Deng, C. Zhao, Z. Li, Biomaterials 91 (2016) 81–89.
[20] Z. Sun, Y. Zhao, Z. Li, H. Cui, Y. Zhou, W. Li, W. Tao, H. Zhang, H. Wang, P.K. Chu, X. Yu, Small 13 (2017) 1602896.
[21] J. Kang, D. Kim, J. Wang, Y. Han, J.M. Zuidema, A. Hariri, J. Park, J.V. Jokerst, M.J. Sailor, Adv. Mater. 30 (2018) 1800512.
[22] J. Zhang, J. Zhang, W. Li, R. Chen, Z. Zhang, W. Zhang, Y. Tang, X. Chen, G. Liu, C. Lee, Theranostics 7 (2017) 3007–3020.
[23] L. Cheng, C. Wang, L.Z. Feng, K. Yang, Z. Liu, Chem. Rev. 114 (2014) 10869–10939.
[24] J. Liu, F. Erogbogbo, K. Yong, L. Ye, J. Liu, R. Hu, H. Chen, Y. Hu, Y. Yang, J. Yang, I. Roy, N.A. Karker, M.T. Swihart, P.N. Prasad, ACS Nano 7 (2013) 7303–7310.
[25] F. Erogbogbo, K. Yong, I. Roy, R. Hu, W. Law, W. Zhao, H. Ding, F. Wu, R. Kumar, M.T. Swihart, P.N. Prasad, ACS Nano 5 (2011) 413–423.
[26] E.R. BERMAN, I.C. MICHAELSON, Exp. Eye Res. 3 (1964) 9–15.
[27] M. Qiu, W.X. Ren, T. Jeong, M. Won, G.Y. Park, D.K. Sang, L. Liu, H. Zhang, J.S. Kim, Chem. Soc. Rev. 47 (2018) 5588–5601.
[28] T. Fan, Y. Zhou, M. Qiu, H. Zhang, J. Innov. Opt. Heal. Sci. (2018) 1830003.
[29] E.J. Anglin, L. Cheng, W.R. Freeman, M.J. Sailor, Adv. Drug Deliv. Rev. 60 (2008) 1266–1277.
[30] F. Erogbogbo, J. May, M. Swihart, P.N. Prasad, K. Smart, S. El Jack, D. Korcyk, M. Webster, R. Stewart, I. Zeng, M. Jullig, K. Bakeev, M. Jamieson, N. Kasabov, B. Gopalan, L. Liang, R. Hu, S. Schliebs, S. Villas-Boas, P. Gladding, Theranostics 3 (2013) 719–728.
[31] A. Castellanos-Gomez, J. Phys. Chem. Lett. 6 (2015) 4280–4291.
[32] W. Tao, X. Zhu, X. Yu, X. Zeng, Q. Xiao, X. Zhang, X. Ji, X. Wang, J. Shi, H. Zhang, L. Mei, Adv. Mater. 29 (2016) 1603276.
[33] H.U. Lee, S.Y. Park, S.C. Lee, S. Choi, S. Seo, H. Kim, J. Won, K. Choi, K.S. Kang, H.G. Park, H.S. Kim, H.R. An, K.H. Jeong, Y.C. Lee, J. Lee, Small 12 (2016) 214–219.
[34] N.M. Latiff, W.Z. Teo, Z. Sofer, A.C. Fisher, M. Pumera, Chem. Eur. J. 21 (2015) 13991–13995.
[35] M. Qiu, Z. Sun, D.K. Sang, X. Han, H. Zhang, C. Niu, Nanoscale 9 (2017) 13384–13403.
[36] L. Li, Y. Yu, G.J. Ye, Q. Ge, X. Ou, H. Wu, D. Feng, X.H. Chen, Y. Zhang, Nature Nanotech. 9 (2014) 372–377.
[37] H. Liu, A.T. Neal, Z. Zhu, Z. Luo, X.F. Xu, D. Tomanek, P. Ye, ACS Nano 8 (2014) 4033–4041.
[38] J. Pei, X. Gai, J. Yang, X. Wang, Z. Yu, D. Choi, B. Luther-Davies, Y. Lu, Nat. Commun. 7 (2016).
[39] J.R. Brent, N. Savjani, E.A. Lewis, S.J. Haigh, D.J. Lewis, P. O'Brien, Chem. Commun. 50 (2014) 13338–13341.
[40] P. Yasaei, B. Kumar, T. Foroozan, C. Wang, M. Asadi, D. Tuschel, J.E. Indacochea, R.F. Klie, A. Salehi-Khojin, Adv. Mater. 27 (2015) 1887–1892.
[41] A.H. Woomer, T.W. Farnsworth, J. Hu, R.A. Wells, C.L. Donley, S.C. Warren, ACS Nano 9 (2015) 8869–8884.
[42] W.C. Zhao, Z.M. Xue, J.F. Wang, J.Y. Jiang, X.H. Zhao, T.C. Mu, ACS Appl. Mater. Inter. 7 (2015) 27608–27612.
[43] X. Tang, W. Liang, J. Zhao, Z. Li, M. Qiu, T. Fan, C.S. Luo, Y. Zhou, Y. Li, Z. Guo, D. Fan, H. Zhang, Small (2017) 1702739.
[44] X. Tang, H. Chen, J.S. Ponraj, S.C. Dhanabalan, Q. Xiao, D. Fan, H. Zhang, Adv. Sci. 0 (2018) 1800420.
[45] J. Kang, S.A. Wells, J.D. Wood, J. Lee, X. Liu, C.R. Ryder, J. Zhu, J.R. Guest, C.A. Husko, M.C. Hersam, Proc. Natl. Acad. Sci. U. S. A. 113 (2016) 11688–11693.
[46] J.B. Smith, D. Hagaman, H.F. Ji, Nanotechnology 27 (2016) 215602.
[47] Y.J. Xu, J. Yuan, L.F. Fei, X.L. Wang, Q.L. Bao, Y. Wang, K. Zhang, Y.G. Zhang, Small 12 (2016) 5000–5007.
[48] Y.Y. Zhang, X.H. Rui, Y.X. Tang, Y.Q. Liu, J.Q. Wei, S. Chen, W.R. Leow, W.L. Li, Y.J. Liu, J.Y. Deng, B. Ma, Q.Y. Yan, X.D. Chen, Adv. Energy Mater. 6 (2016) 1502409.
[49] W.L. Wilson, P.F. Szajowski, L.E. Brus, Science 262 (1993) 1242–1244.
[50] X. Ji, H. Wang, B. Song, B. Chu, Y. He, Front. Chem. 6 (2018) 00038.
[51] C.S. Yang, R.A. Bley, S.M. Kauzlarich, H. Lee, G.R. Delgado, J. Am. Chem. Soc. 121 (1999) 5191–5195.
[52] X.G. Li, Y.Q. He, S.S. Talukdar, M.T. Swihart, Langmuir 19 (2003) 8490–8496.
[53] L. Mangolini, E. Thimsen, U. Kortshagen, Nano Lett. 5 (2005) 655–659.
[54] C.M. Hessel, E.J. Henderson, J.G.C. Veinot, Chem. Mater. 18 (2006) 6139–6146.
[55] J. Park, L. Gu, G. von Maltzahn, E. Ruoslahti, S.N. Bhatia, M.J. Sailor, Nat. Mater. 8 (2009) 331–336.
[56] S.J.P. McInnes, N.H. Voelcker, Future Med. Chem. 1 (2009) 1051–1074.
[57] M.J. Sailor, Porous Silicon in Practice: Preparation, Characterization and Applications, John Wiley & Sons (2013).
[58] A. Kashyout, H.M.A. Soliman, M. Nabil, A.A. Bishara, Mater. Lett. 100 (2013) 184–187.
[59] A.V. Kabashin, P. Delaporte, A. Pereira, D. Grojo, R. Torres, T. Sarnet, M. Sentis, Nanoscale Res. Lett. 5 (2010) 454–463.
[60] Q. Zhou, Q. Chen, Y. Tong, J. Wang, Angew. Chemie Int. Ed. 55 (2016) 11437–11441.
[61] Y. Zhao, H. Wang, H. Huang, Q. Xiao, Y. Xu, Z. Guo, H. Xie, J. Shao, Z. Sun, W. Han, X. Yu, P. Li, P.K. Chu, Angew. Chemie Int. Ed. English 55 (2016) 5003–5007.
[62] C.R. Ryder, J.D. Wood, S.A. Wells, Y. Yang, D. Jariwala, T.J. Marks, G.C. Schatz, M.C. Hersam, Nat. Chem. 8 (2016) 598–603.
[63] G. Qu, W. Liu, Y. Zhao, J. Gao, T. Xia, J. Shi, L. Hu, W. Zhou, J. Gao, H. Wang, Q. Luo, Q. Zhou, S. Liu, X. Yu, G. Jiang, Angew. Chemie Int. Ed. English (2017) 14488–14493.
[64] Y. Zhao, L. Tong, Z. Li, N. Yang, H. Fu, L. Wu, H. Cui, W. Zhou, J. Wang, H. Wang, P.K. Chu, X. Yu, Chem. Mater. 29 (2017) 7131–7139.
[65] N.K. Hon, Z. Shaposhnik, E.D. Diebold, F. Tamanoi, B. Jalali, J. Biomed. Mater. Res. A. 100A (2012) 3416–3421.
[66] X.G. Li, Y.Q. He, M.T. Swihart, Langmuir 20 (2004) 4720–4727.
[67] S. Sato, M.T. Swihart, Chem. Mater. 18 (2006) 4083–4088.
[68] F. Erogbogbo, C. Tien, C. Chang, K. Yong, W. Law, H. Ding, I. Roy, M.T. Swihart, P.N. Prasad, Bioconjugate Chem. 22 (2011) 1081–1088.
[69] Y. Su, X. Ji, Y. He, Adv. Mater. 28 (2016) 10567–10574.
[70] F. Erogbogbo, K. Yong, R. Hu, W. Law, H. Ding, C. Chang, P.N. Prasad, M.T. Swihart, ACS Nano 4 (2010) 5131–5138.
[71] F. Erogbogbo, X. Liu, J.L. May, A. Narain, P. Gladding, M.T. Swihart, P.N. Prasad, Integr Biol-Uk 5 (2013) 144–150.
[72] W.Y. So, Q. Li, C.M. Legaspi, B. Redler, K.M. Koe, R. Jin, L.A. Peteanu, ACS Nano 12 (2018) 7232–7238.
[73] Q. Li, T. Luo, M. Zhou, H. Abroshan, J. Huang, H.J. Kim, N.L. Rosi, Z. Shao, R. Jin, ACS Nano 10 (2016) 8385–8393.
[74] M. Dasog, Z. Yang, S. Regli, T.M. Atkins, A. Faramus, M.P. Singh, E. Muthuswamy, S.M. Kauzlarich, R.D. Tilley, J.G.C. Veinot, ACS Nano 7 (2013) 2676–2685.
[75] R. Sinelnikov, M. Dasog, J. Beamish, A. Meldrum, J.G.C. Veinot, ACS Photonics 4 (2017) 1920–1929.
[76] M. Dasog, J. Kehrle, B. Rieger, J.G.C. Veinot, Angew. Chemie Int. Ed. English 55 (2016) 2322–2339.
[77] F. Hua, M.T. Swihart, E. Ruckenstein, Langmuir 21 (2005) 6054–6062.
[78] J. Liu, F. Erogbogbo, K. Yong, L. Ye, J. Liu, R. Hu, H. Chen, Y. Hu, Y. Yang, J. Yang, I. Roy, N.A. Karker, M.T. Swihart, P.N. Prasad, ACS Nano 7 (2013) 7303–7310.
[79] D. Jurbergs, E. Rogojina, L. Mangolini, U. Kortshagen, Appl. Phys. Lett. 88 (2006) 233116.
[80] Y. Yu, G. Fan, A. Fermi, R. Mazzaro, V. Morandi, P. Ceroni, D. Smilgies, B.A. Korgel, J. Phys. Chem. C 121 (2017) 23240–23248.
[81] A. Marinins, R. Zandi Shafagh, W. van der Wijngaart, T. Haraldsson, J. Linnros, J.G.C. Veinot, S. Popov, I. Sychugov, ACS Appl. Mater. Inter. 9 (2017) 30267–30272.
[82] M. Qiu, D. Wang, W. Liang, L. Liu, Y. Zhang, X. Chen, D.K. Sang, C. Xing, Z. Li, B. Dong, Proc. Natl. Acad. Sci. U. S. A. 115 (2018) 501–506.
[83] J. Mo, Q. Xie, W. Wei, J. Zhao, Nat. Commun. 9 (2018) 2480.
[84] X. Zhang, Z. Zhang, S. Zhang, D. Li, W. Ma, C. Ma, F. Wu, Q. Zhao, Q. Yan, B. Xing, Small 13 (2017) 1701210.
[85] T. Baati, A. Al-Kattan, M. Esteve, L. Njim, Y. Ryabchikov, F. Chaspoul, M. Hammami, M. Sentis, A.V. Kabashin, D. Braguer, Sci Rep-Uk 6 (2016) 25400.
[86] S. Bhattacharjee, L.H.J. de Haan, N.M. Evers, X. Jiang, A.T.M. Marcelis, H. Zuilhof, I.M.C.M. Rietjens, G.M. Alink, Part. Fibre Toxicol. 7 (2010) 7–25.
[87] A. Shiohara, S. Hanada, S. Prabakar, K. Fujioka, T.H. Lim, K. Yamamoto, P.T. Northcote, R.D. Tilley, J. Am. Chem. Soc. 132 (2010) 248–253.
[88] F. Erogbogbo, K. Yong, I. Roy, R. Hu, W. Law, W. Zhao, H. Ding, F. Wu, R. Kumar, M.T. Swihart, P.N. Prasad, ACS Nano 5 (2011) 413–423.
[89] J. Liu, M. Yu, C. Zhou, S. Yang, X. Ning, J. Zheng, J. Am. Chem. Soc. 135 (2013) 4978–4981.
[90] G. Song, J. Hao, C. Liang, T. Liu, M. Gao, L. Cheng, J. Hu, Z. Liu, Angew. Chemie Int. Ed. English 55 (2016) 2122–2126.
[91] F. Erogbogbo, C. Tien, C. Chang, K. Yong, W. Law, H. Ding, I. Roy, M.T. Swihart, P.N. Prasad, Bioconjugate Chem. 22 (2011) 1081–1088.
[92] A. Al-Kattan, Y.V. Ryabchikov, T. Baati, V. Chirvony, J.F. Sanchez-Royo, M. Sentis, D. Braguer, V.Y. Timoshenko, M. Esteve, A.V. Kabashin, J. Mater. Chem. B Mater. Biol. Med. 4 (2016) 7852–7858.
[93] X. Zhang, M. Brynda, R.D. Britt, E.C. Carroll, D.S. Larsen, A.Y. Louie, S.M. Kauzlarich, J. Am. Chem. Soc. 129 (2007) 10668–10669.
[94] C. Tu, X. Ma, P. Pantazis, S.M. Kauzlarich, A.Y. Louie, J. Am. Chem. Soc. 132 (2010) 2016–2023.
[95] F. Erogbogbo, C. Chang, J.L. May, L. Liu, R. Kumar, W. Law, H. Ding, K.T. Yong, I. Roy, M. Sheshadri, M.T. Swihart, P.N. Prasad, Nanoscale 4 (2012) 5483–5489.
[96] S. Yan, B. Wang, Z. Wang, D. Hu, X. Xu, J. Wang, Y. Shi, Biosens. Bioelectron. 80 (2016) 34–38.
[97] V. Kumar, J.R. Brent, M. Shorie, H. Kaur, G. Chadha, A.G. Thomas, E.A. Lewis, A.P. Rooney, L. Nguyen, X.L. Zhong, M.G. Burke, S.J. Haigh, A. Walton, P.D. McNaughter, A.A. Tedstone, N. Savjani, C.A. Muryn, P.O. Brien, A.K. Ganguli, D.J. Lewis, P. Sabherwal, ACS Appl. Mater. Inter. 8 (2016) 22860–22868.
[98] C.C. Mayorga-Martinez, N. Mohamad Latiff, A.Y.S. Eng, Z. Sofer, M. Pumera, Anal. Chem. 88 (2016) 10074–10079.
[99] T.Y. Ying, Z. Sofer, C.C. Mayorgamartinez, M. Pumera, Mater. Chem. (2017) 1130–1136.
[100] W. Gu, Y. Yan, X. Pei, C. Zhang, C. Ding, Y. Xian, Sens. Actuators B Chem. 250 (2017) 601–607.
[101] J. Peng, Y.Q. Lai, Y.Y. Chen, J. Xu, L.P. Sun, J. Weng, Small 13 (2017).
[102] J. Zhou, Z. Li, M. Ying, M. Liu, X. Wang, X. Wang, L. Cao, H. Zhang, G. Xu, Nanoscale 10 (2018) 5060–5064.
[103] Y. Cui, Q.Q. Wei, H.K. Park, C.M. Lieber, Science 293 (2001) 1289–1292.
[104] F. Patolsky, B.P. Timko, G. Yu, Y. Fang, A.B. Greytak, G. Zheng, C.M. Lieber, Science 313 (2006) 1100–1104.
[105] Y. Yi, J. Deng, Y. Zhang, H. Li, S. Yao, Chem. Commun. 49 (2013) 612–614.

[106] B. Chu, B. Song, X. Ji, Y. Su, H. Wang, Y. He, Anal. Chem. 89 (2017) 12152–12159.
[107] Y. He, C. Fan, S. Lee, Nano Today 5 (2010) 282–295.
[108] W. Chen, J. Ouyang, H. Liu, M. Chen, K. Zeng, J. Sheng, Z. Liu, Y. Han, L. Wang, J. Li, L. Deng, Y. Liu, S. Guo, Adv. Mater. 29 (2016) 1603864.
[109] X. Ji, F. Peng, Y. Zhong, Y. Su, X. Jiang, C. Song, L. Yang, B. Chu, S. Lee, Y. He, Adv. Mater. 27 (2015) 1029–1034.
[110] F. Yin, K. Hu, S. Chen, D. Wang, J. Zhang, M. Xie, D. Yang, M. Qiu, H. Zhang, Z. Li, J. Mater. Chem. B Mater. Biol. Med. 5 (2017) 5433–5440.
[111] J. Shen, R. Xu, J. Mai, H. Kim, X. Guo, G. Qin, Y. Yang, J. Wolfram, C. Mu, X. Xia, J. Gu, X. Liu, Z. Mao, M. Ferrari, H. Shen, ACS Nano 7 (2013) 9867–9880.
[112] W. Chen, J. Ouyang, X. Yi, Y. Xu, C. Niu, Adv. Mater. (2017) 1703458.
[113] D. Guo, X. Ji, H. Wang, B. Sun, B. Chu, Y. Shi, Y. Su, Y. He, J. Mater. Chem. B Mater. Biol. Med. 6 (2018) 3876–3883.
[114] Y. Li, Z. Liu, Y. Hou, G. Yang, X. Fei, H. Zhao, Y. Guo, C. Su, Z. Wang, H. Zhong, ACS Appl. Mater. Inter. (2017) 25098–25106.
[115] G. Yang, Z. Liu, Y. Li, Y. Hou, X. Fei, C. Su, S. Wang, Z. Zhuang, Z. Guo, Biomater. Sci. 5 (2017) 2048–2055.
[116] C. Lee, H.S. Hwang, S. Lee, B. Kim, J.O. Kim, K.T. Oh, E.S. Lee, H.G. Choi, Y.S. Youn, Adv. Mater. 29 (2017) 1605563.

Meng Qiu received his PhD from Institute of Chemistry, Chinese Academy of Sciences in 2013. He joined Prof. Han Zhang's lab in Shenzhen University as a research fellow, and then joined Prof. Jong Seung Kim in Korea University as a research professor. His research interests focus on the design and synthesis of two-dimensional materials for biomedical applications.

Ajay Singh obtained his Ph.D. from the partnership program of Department of Organic & Nano System Engineering, Konkuk University, India, and the Center for Theragnosis, Korea Institute of Science and Technology (KIST), Korea in 2013. He was a postdoctoral associate in KIST , and later , a research assistant professor at the Institute for Lasers, Photonics, and Biophotonics, University at Buffalo, State University of New York . Unfortunately, he passed away on Oct. 20, 2018. His research interests were in theranostic materials for molecular imaging, nanomedicine, and drug delivery.

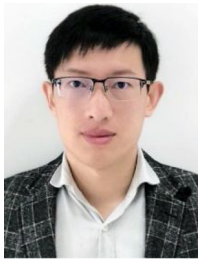

Dou Wang obtained his Ph.D. in Biochemistry and Molecular Biology from the University of Chinese Academy of Sciences in 2016. He is currently an Assistant Professor at Jinan University. His research interests include development of novel nanomaterials as drug delivery systems for cancer treatment and nanotechnology for early diagnosis of diseases.

Junle Qu received his PhD degree from the Department Xi'an Institute of Optics and Precision Mechanics, Chinese Academy of Sciences in 1998. He is currently a professor in the College of Optoelectronic Engineering at Shenzhen University. His research focuses on cutting-edge biomedical optical imaging techniques including FLIM, super-resolution and non-linear optical techniques and their application in monitoring cell processes and cell–drug interactions.

Mark Swihart is a UB Distinguished Professor , and the Chair of the department of Chemical and Biological Engineering at the State University of New York. He earned his Ph.D. in chemical engineering from the University of Minnesota in 1997, followed by one year of postdoctoral research in mechanical engineering at the University of Minnesota. His research interests are in the synthesis and processing of inorganic nanomaterials for applications ranging from energy harvesting and conversion to nanomedicine. He has received awards from the American Chemical Society and the Electrochemical Society.

Han Zhang received his B.S. degree from Wuhan University in 2006 and PhD from Nanyang Technological University in 2010. He is currently a director of Shenzhen Key Laboratory of 2D Materials and Devices, and Shenzhen Engineering Laboratory of Phosphorene and Optoelectronics, Shenzhen University. To date, he has published over 203 scientific publications and 38 patents. His current research focus is the ultrafast and nonlinear photonics of two-dimensional materials.

Paras N. Prasad is a SUNY Distinguished Professor of Chemistry, Physics, Electrical Engineering and Medicine; the Samuel P. Capen Chair of Chemistry; the Executive Director of Institute for Lasers, Photonics, and Biophotonics, University at Buffalo, The State University of New York. He was named among top 50 science and technology leaders in the world by Scientific American in 2005. He has published over 800 scientific and technical papers, four monographs and eight edited books. He has received many scientific awards and honors. His interests include biophotonics, nanophotonics, nanomedicine, metamaterials, and solar cells.